# NAVAL POSTGRADUATE SCHOOL
## Monterey, California


# THESIS

**SIMULATIONS OF A SHORT RAYLEIGH LENGTH 100 kW FEL AND MIRROR STABILITY ANALYSIS**

by

Thomas E. Campbell

December 2002

| | |
|---|---|
| Thesis Advisor: | William B. Colson |
| Second Reader: | Robert L. Armstead |

**Approved for public release; distribution unlimited**

THIS PAGE INTENTIONALLY LEFT BLANK

| REPORT DOCUMENTATION PAGE | | | Form Approved OMB No. 0704-0188 |
|---|---|---|---|
| Public reporting burden for this collection of information is estimated to average 1 hour per response, including the time for reviewing instruction, searching existing data sources, gathering and maintaining the data needed, and completing and reviewing the collection of information. Send comments regarding this burden estimate or any other aspect of this collection of information, including suggestions for reducing this burden, to Washington headquarters Services, Directorate for Information Operations and Reports, 1215 Jefferson Davis Highway, Suite 1204, Arlington, VA 22202-4302, and to the Office of Management and Budget, Paperwork Reduction Project (0704-0188) Washington DC 20503. | | | |
| **1. AGENCY USE ONLY** ***(Leave blank)*** | **2. REPORT DATE** December 2002 | **3. REPORT TYPE AND DATES COVERED** Master's Thesis | |
| **4. TITLE AND SUBTITLE**: Simulations of a Short Rayleigh Length 100 kW FEL and Mirror Stability Analysis | | | **5. FUNDING NUMBERS** |
| **6. AUTHOR(S) Campbell, Thomas E.** | | | |
| **7. PERFORMING ORGANIZATION NAME(S) AND ADDRESS(ES)** Naval Postgraduate School Monterey, CA 93943-5000 | | | **8. PERFORMING ORGANIZATION REPORT NUMBER** |
| **9. SPONSORING /MONITORING AGENCY NAME(S) AND ADDRESS(ES)** N/A | | | **10. SPONSORING/MONITORING AGENCY REPORT NUMBER** |
| **11. SUPPLEMENTARY NOTES** The views expressed in this thesis are those of the author and do not reflect the official policy or position of the Department of Defense or the U.S. Government. | | | |
| **12a. DISTRIBUTION / AVAILABILITY STATEMENT** Approved for public release; distribution unlimited | | | **12b. DISTRIBUTION CODE** |


**13. ABSTRACT** ***(maximum 200 words)***

A MW class free electron laser capable of delivering energy at the speed of light can improve ASCM defensive capability for Navy ships. Many design challenges must be overcome to make such a weapon possible. One such challenge is to maintain the power density on laser cavity mirrors at acceptable levels. The use of a short Rayleigh length to increase beam spot size at the mirror is studied as a possible solution to this problem. In this thesis, it is shown that by using a short Rayleigh length FEL, power densities at the mirrors are significantly reduced without causing a noticeable reduction in performance.

For a short Rayleigh length FEL, the resonator cavity is sensitive to misalignment and vibration. The effect of mirror tilt due to vibrations is explored and the results show that as mirror tilt increases, FEL efficiency does decreases. However, a mirror tilt several orders of magnitude greater than currently achievable active alignment tolerances is required before the FEL efficiency is noticeably affected. In this thesis, it is shown that mirror tilt within achievable tolerance limits will not adversely affect the performance of a FEL.


| **14. SUBJECT TERMS** Free Electron Laser, short Rayleigh length, mirror stability | | | **15. NUMBER OF PAGES** 102 |
|---|---|---|---|
| | | | **16. PRICE CODE** |
| **17. SECURITY CLASSIFICATION OF REPORT** Unclassified | **18. SECURITY CLASSIFICATION OF THIS PAGE** Unclassified | **19. SECURITY CLASSIFICATION OF ABSTRACT** Unclassified | **20. LIMITATION OF ABSTRACT** UL |

NSN 7540-01-280-5500 Standard Form 298 (Rev. 2-89)
Prescribed by ANSI Std. 239-18

THIS PAGE INTENTIONALLY LEFT BLANK

**Approved for public release; distribution unlimited**

**SIMULATIONS OF A SHORT RAYLEIGH LENGTH 100 kW FEL AND MIRROR STABILITY ANALYSIS**

Thomas E. Campbell
Lieutenant, United States Navy
B.S., Auburn University, 1995

Submitted in partial fulfillment of the
requirements for the degree of

**MASTER OF SCIENCE IN PHYSICS**

from the

**NAVAL POSTGRADUATE SCHOOL**
**December 2002**

Author: Thomas E. Campbell

Approved by: William B. Colson
Thesis Advisor

Robert L. Armstead
Second Reader/Co-Advisor

William Maier II
Chairman, Department of Physics

THIS PAGE INTENTIONALLY LEFT BLANK

# ABSTRACT

A MW class free electron laser capable of delivering energy at the speed of light can improve ASCM defensive capability for Navy ships. Many design challenges must be overcome to make such a weapon possible. One such challenge is to maintain the power density on laser cavity mirrors at acceptable levels. The use of a short Rayleigh length to increase beam spot size at the mirror is studied as a possible solution to this problem. In this thesis, it is shown that by using a short Rayleigh length FEL, power densities at the mirrors are significantly reduced without causing a noticeable reduction in performance.

For a short Rayleigh length FEL, the resonator cavity is sensitive to misalignment and vibration. The effect of mirror tilt due to vibrations is explored and the results show that as mirror tilt increases, FEL efficiency does decreases. However, a mirror tilt several orders of magnitude greater than currently achievable active alignment tolerances is required before the FEL efficiency is noticeably affected. In this thesis, it is shown that mirror tilt within achievable tolerance limits will not adversely affect the performance of a FEL.

THIS PAGE INTENTIONALLY LEFT BLANK

# TABLE OF CONTENTS

# LIST OF FIGURES

THIS PAGE INTENTIONALLY LEFT BLANK

# LIST OF TABLES

THIS PAGE INTENTIONALLY LEFT BLANK

# ACKNOWLEDGMENTS

I would like to take this opportunity to thank Professor Colson for his guidance and patience while teaching me about free electron lasers, and helping me complete this thesis. This has been a great experience both academically, and professionally.

I would also like to thank Professor Crooker, and Professor Armstead, for all the helpful suggestions and comments; your time and efforts in proofreading my thesis are greatly appreciated. Thank you Professor Blau for all your help while here at NPS. Alan Todd at Advanced Energy Systems, and George Neil at JLAb, thank you for all of your inputs and help.

To the cave dwellers in the basement, thanks for all the good times. Bill Ossenfort, thank you for all the help and great times. WAR EAGLE!!!

I thank my wife Gina for all of her support and sacrifices that she has made during my career. With out you, none of this would have been possible. I love you. To my three beautiful daughters, Lauren, Emily and Hannah – thank you for all the hugs and love, you have made the time here more special than you will ever know.

Finally, I thank God for all the blessings in my life and for the opportunities that I have been given.

THIS PAGE INTENTIONALLY LEFT BLANK

# LIST OF SYMBOLS

| | |
|---|---|
| $\vec{B}$ | vector sum of the undulator and optical magnetic fields |
| $\vec{B}_s$ | optical magnetic field |
| $\vec{B}_u$ | undulator magnetic field |
| $c$ | speed of light |
| $C$ | specific heat |
| $e$ | charge of an electron |
| $E_e$ | electron energy |
| $E_{las}$ | accelerator output energy |
| $E_{melt}$ | energy required to melt 500 $cm^3$ of Al |
| $\vec{E}_s$ | optical electric field |
| $(DE/L)_{acc}$ | acceleration gradient |
| h | Plank's constant |
| $I_{avg}$ | average FEL current |
| $I_{pk}$ | peak FEL current |
| $k$ | optical wave number |
| $k_0$ | undulator magnetic wave number |
| $K$ | undulator parameter |
| $L$ | undulator length |
| $H_m$ | latent heat of melting for Al |
| $m_e$ | mass of an electron |
| $N$ | number of undulator magnetic periods |
| $P$ | optical power at a range |
| $P_e$ | power radiated by an electron |
| $P_{out}$ | optical power out |
| $q$ | bunch charge |
| $S$ | resonator length |
| $t$ | time |
| $T_m$ | melting temperature |
| $T_0$ | initial temperature |
| $\vec{v}_e$ | electron velocity through the FEL cavity |
| $V$ | volume |
| $V_{gun}$ | injector gun voltage |
| $a$ | extinction coefficient, fine structure constant |
| $\vec{b}$ | non-dimensional electron velocity |
| $b_\perp$ | transverse component of $\vec{b}$ |
| $b_z$ | axial component of $\vec{b}$ |
| $g$ | Lorentz factor |
| $Dg/g$ | electron energy spread |

| | |
|---|---|
| $l_0$ | magnetic period length |
| $l$ | optical wave length |
| $h$ | undulator extraction efficiency |
| $h_{rf}$ | accelerator efficiency |
| $f$ | initial optical phase |
| $r$ | density |
| $y$ | optical phase |
| $w_{mirror}$ | optical spot radius at cavity mirror |
| $z$ | electron phase |
| $a$ | dimensionless optical field |
| $E_s$ | optical field amplitude |
| $e_{rms}$ | rms electron beam emittance |
| $e_N$ | normalized electron beam emittance |
| $F$ | dimensionless filling factor |
| $G$ | optical field single-pass gain |
| $J$ | current density |
| $j$ | dimensionless current density |
| $k$ | optical wavenumber |
| $k_0$ | undulator wavenumber |
| $L$ | undulator length |
| $l_e$ | electron pulse length |
| $n$ | number of passes through the undulator |
| $Q$ | resonator quality factor |
| $r_e$ | electron beam radius |
| $r_m$ | dimensionless mirror radius |
| $r_c$ | dimensionless radius of curvature |
| $\tau$ | dimensionless time |
| $W$ | pulse repetition rate |
| $W_0$ | optical mode radius |
| $w_0$ | dimensionless optical waist radius |
| $Z_0$ | Rayleigh length |
| $z_0$ | dimensionless Rayleigh length |
| $s_x$ | dimensionless electron beam radius in x direction |
| $s_y$ | dimensionless electron beam radius in y direction |
| $s_{qx}$ | electron beam angular spread in x direction |
| $s_{qy}$ | electron beam angular spread in y direction |
| $v$ | electron beam phase velocity |
| $z$ | electron beam phase |

# LIST OF ACRONYMS

| | |
|---|---|
| ABL | Airborne Laser |
| ASCM | Anti-Ship Cruise Missile |
| CIWS | Close-In Weapons System |
| COIL | Chemical Oxygen Iodine Laser |
| FAS | Federation of American Scientists |
| FEL | Free Electron Laser |
| FY | Fiscal Year |
| GAO | Government Accounting Office |
| HEL | High Energy Laser |
| HV | High Voltage |
| IR | Infrared |
| MIRACL | Mid-Infrared Advanced Chemical Laser |
| PRF | Pulse Repetition Frequency |
| RAM | Rolling Airframe Missile |
| RF | Radio Frequency |
| THEL | Tactical High Energy Laser |
| TJNAF | Thomas Jefferson National Accelerator Facilities |
| SRF | Superconducting Radio Frequency |
| UV | Ultra Violet |

THIS PAGE INTENTIONALLY LEFT BLANK

# I. INTRODUCTION

The U.S. Navy's interest in a high energy laser was expressed by the Commander in Chief of the U.S. Atlantic Fleet on the 24th of April, 2001, in a letter to the Chief of Naval Operations:

> …that the Speed of Light weapons can be very effective against these small high speed threats. Such a laser weapon would offer our Naval forces an extremely versatile weapon to counter numerous soft and hard targets. A High Energy Laser weapon can be designed to deliver energy that can track, warn, damage, mission kill, and if need be, destroy a threat. I believe it is exactly this type of weapon system that our forces need in the littoral environment where, even though the threat may not be as sophisticated as a highly maneuverable cruise missile….

The free electron laser (FEL) is a possible answer for the Navy's desire for a high energy laser (HEL) weapon system. Chapter II of this thesis presents background information on why directed energy weapons, and specifically the FEL, are a possible choice as an anti-ship cruise missile defense system.

Chapter III gives a detailed description of the Thomas Jefferson Nuclear Accelerator Facilities (TJNAF) proposed 100 kW FEL. The description includes a brief overview of FEL components and the parameters used for this particular design.

Chapter IV presents a basic overview of FEL theory and physics required to understand the operations of a FEL. The description of how energy is transferred from the electron beam to the laser beam is presented along with the supporting theory and equations.

Chapter V presents simulation results of short Rayleigh length FEL's. A short Rayleigh length FEL is explored as a possible method to decrease the power density on laser cavity optical mirrors, thus preventing mirror damage. Due to the large number of simulations required for this research, the work was divided among several people with my contribution consisting of simulations and analysis for Rayleigh lengths of $Z_0$ = 0 1L and 0.2L where L is the undulator length. This material was originally presented at the

23rd International FEL Conference in Darmstadt Germany in August 2001 and has been published in Nuclear Instruments and Methods in Physics Research [1].

Chapter VI presents simulation results describing stability analysis of the FEL when operating with a slight mirror tilt. This is the first such study of the effect of mirror tilt on the performance of the FEL. For an FEL using a short Rayleigh length, the optical mode may be sensitive to mirror tilt angle due to vibrations. Multiple simulations were conducted to determine the actual affect on FEL performance. Again, due to the large number of simulations, the work was divided among several people, with my contribution consisting of simulation and analysis of data for mirror tilt angles from 0 to 400 ìrad. This material was originally presented at the 24th International FEL Conference in Chicago, Illinois in September 2002, and will be published in 2003

Chapter VII presents an analysis to determine the required power for a shipboard point defense system FEL. Target kill mechanisms, and atmospheric propagation losses are considered to show that a MW class FEL has the potential to be a successful ASCM point defense system.

# II. BACKGROUND

## A. WHY DIRECTED ENERGY

Since the end of the Cold War, the U.S. Navy's focus has shifted from preparing for warfare on the open ocean to developing capabilities for conducting combat operations in the littoral waters of the world. The proliferation of increasingly sophisticated anti-ship cruise missiles (ASCM's) threatens the ability of Navy ships to operate and survive close to hostile shores. These missiles are low cost weapons that can inflict serious damage to a ship, and must be accounted for in the ship's defensive capabilities.

Current anti-ship missile defense systems include the Phalanx close-in weapons system (CIWS), RIM-116A rolling airframe missile (RAM), and standard missile. These systems provide some measure of defense for the ship against ASCM's, but they have limitations that make ships vulnerable to anti-ship missile attacks. These systems are based on gunnery and rocketry, and have a time of flight required to get to the incoming threat and destroy it. There are a limited number of weapons available in the magazine for use, and once they are depleted the ship is defenseless. The limit of defensive capabilities with these types of defensive weapons is rapidly being approached while the technology for ASCM's has continued to advance. Short range detection of high-speed threat missiles may result in the missiles being destroyed in close proximity to the ship. Destroying the missile minimizes damage to the ship, but missile fragments may strike the ship and cause significant damage to unprotected equipment and personnel. Figure 1 shows the probability of missile fragments hitting the ship as a function of range. For this simulation, a typical missile traveling at 400 m/s at an altitude of 8 m with a spread of missile fragment sizes based on known missile break up from weapons testing is used.

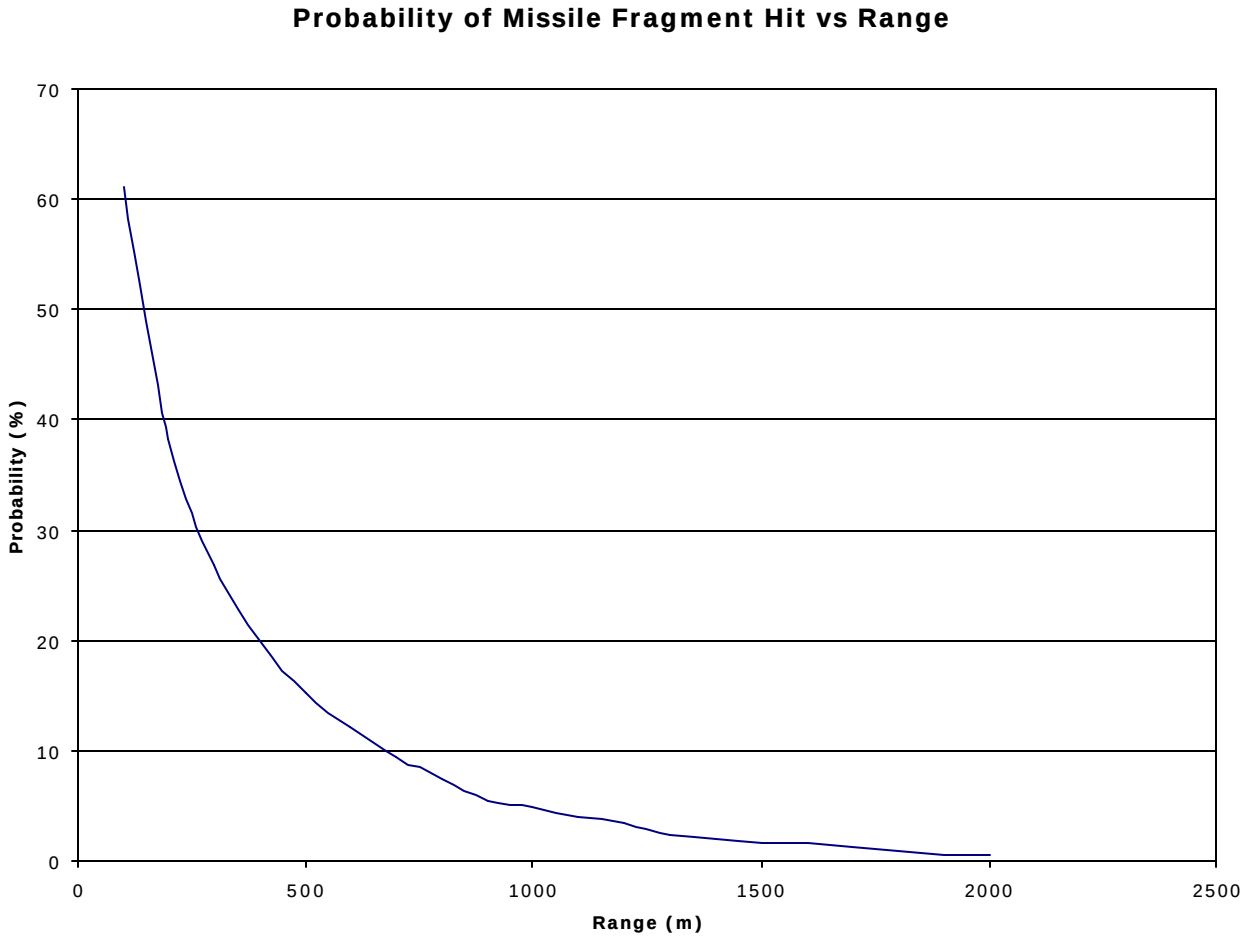


Figure 1. Probability of Missile Fragment Hitting Ship

ASCM's have become faster and more maneuverable, greatly increasing the risk to US warships. The Russian SS-N-26 Oniks is a Mach 3.5 sea skimming ASCM and is an example of velocities representative of these new threat missiles [2]. As the speed of the threat missile increases, the reaction time a ship has to identify an incoming threat, track, develop a solution, and launch a defensive weapon gets shorter. These faster ASCM's and shorter detection ranges are stressing current defense systems to their limit and the only way to keep up with the threat is to pursue new technologies that offer the advantages of faster speed. One such technology currently being considered is directed energy weapons. Directed energy in the form of a laser offers "speed of light" capability and the ability to put large amounts of power onto an incoming missile in a short amount of time, destroying the target at greater ranges than current weapons systems. Several

laser weapons systems are currently in various stages of research and development. The airborne laser program (ABL), and tactical high energy laser (THEL) systems are examples of current projects designed for airborne and ground based applications. Applying this technology would greatly enhance the Navy's ability to defend against high end ASCM's. A closer review of current ship missile defense systems will show that a directed energy weapon system will be a positive asset.

### 1. Phalanx Close –In Weapons System (CIWS)

The Phalanx close-in weapons system, shown in Figure 2 is a rapid-fire 20mm M-61A1 Gatling gun, which is capable of firing up to 4500 rounds/min of depleted uranium or tungsten armor piercing penetrators at a velocity of 1030 m/s [3a.]. The CIWS is a self-contained unit that can search, detect, track, and engage targets, but is typically integrated into a ships combat systems suite for additional fire control capability.

Figure 2. Phalanx Weapons System (from [10])

The Phalanx weapon system is effective only at extremely short-range engagements, typically on the order of 1000 meters or less. The weapon can be fired for a limited amount of time before the barrels begin to overheat; so that the engagement

time for an incoming missile is limited to about five seconds or less. At the firing rate of 4500 shots/min, only 375 bullets are fired at the oncoming missile. Additionally, the magazine only holds 1550 rounds and requires several hours of time out of service to reload [3a.]. Another problem associated with CIWS is its availability. Average operational availability of CIWS averaged 75% on Navy ships for FY 97, 98, and 99 [5]. That means that 25% of the time a ship would be without its last line of defense against an ASCM. While a small magazine and limited firing time are significant, the biggest disadvantage of the CIWS is that most of the shots fired will not hit the incoming missile due to the slight dispersion in bullet trajectories from the gun. This small dispersion angle translates to a large error down range; as a result, most of the shots miss the incoming target. Figure 3 shows a typical bullet dispersion pattern at a range of 1000 meters.

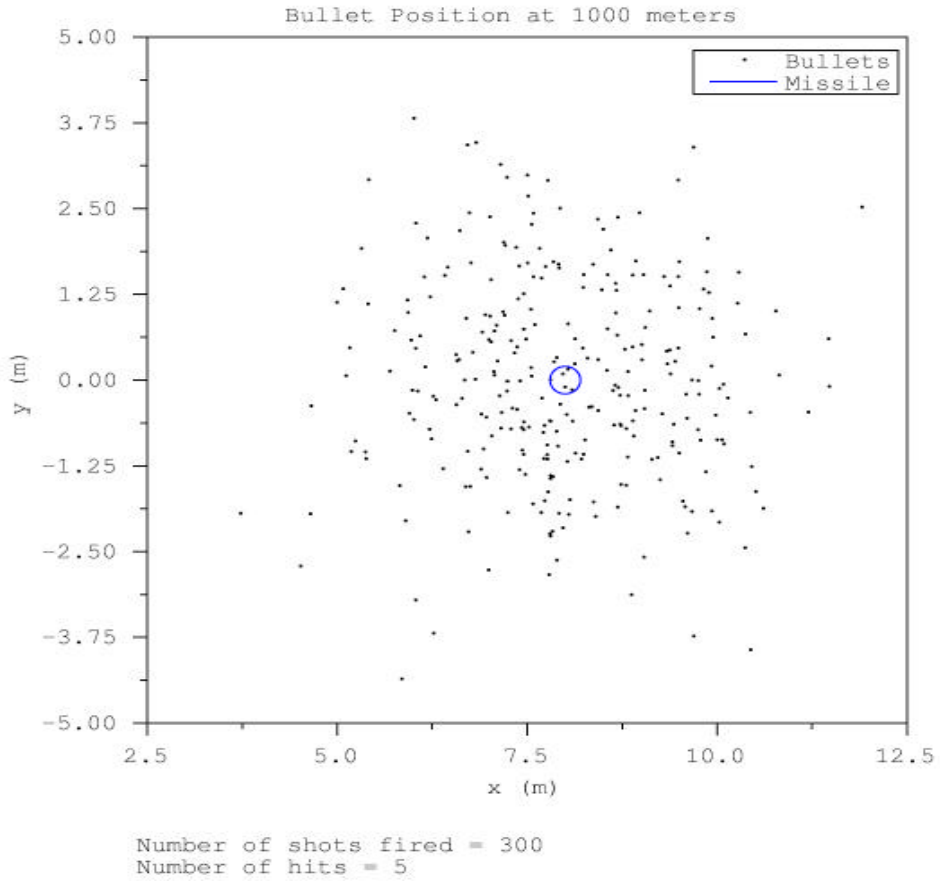


Figure 3. Phalanx Bullet Dispersion at 1000 Meters

For the simulation shown, a total of 300 bullets were fired with a total of 5 hitting on a typical missile cross section of 20 centimeters. This equates to a 1.66 % hit probability at a range of only 1000 meters. The probability of hitting an incoming missile decreases rapidly as range increases. A plot of probability versus range is shown in Figure 4.

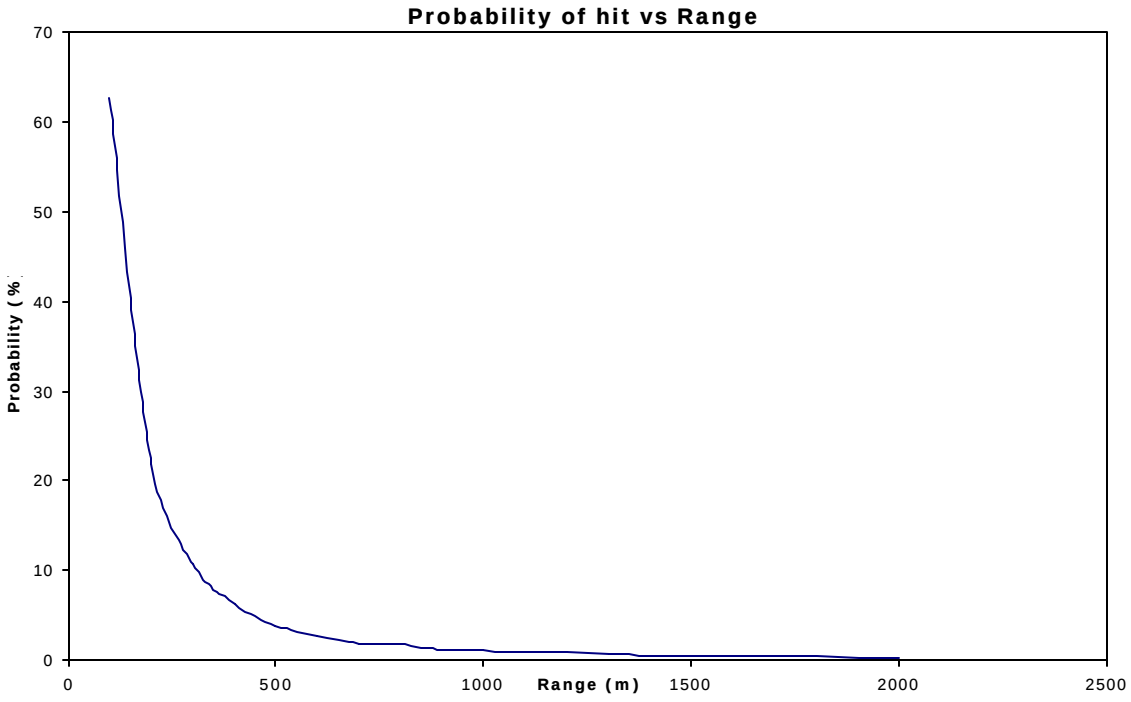


Figure 4. Probability of Hit vs Range for a Single Bullet

Lethality testing shows that destruction of a cruise missile requires multiple hits. The first step in determining the number of hits taken by a missile during its approach is to estimate the number of bullets that the missile will encounter in a 100-meter range of its flight path. Assuming a missile velocity of 400 m/s and a 75 shot/sec firing rate for the gun, the bullets encountered in each 100 meter section of path is calculated to be 26 bullets.

Using the predicted hit probabilities versus range and the number of bullets encountered in 100 meter increments, the typical kill range can be determined. Assuming

it takes an average of 6 hits to "kill" a missile, then a typical range at which a missile will be destroyed is about 400 meters. The destroyed missile may break up into several smaller fragments, each of which could have sufficient kinetic energy to strike the ship and cause significant damage to personnel and unprotected equipment such as radar and antennae. The CIWS is the current last line of defense against ASCM's employed by many US warships. Based on limited engagement time, small magazine capacity, low probability of killing a missile at ranges outside of 500 meters, and high probability of damage from missile debris, the CIWS ability to defend a ship against technologically improved missiles is rapidly diminishing. A directed energy weapon would improve engagement range and remove the dispersion problems encountered by the Phalanx weapon system

### 2. Rolling Airframe Missile (RAM)

The RAM is a point defense weapon system designed to engage a threat missile at intercept ranges out to 9.6 km [3b.]. It utilizes a Mach 2 missile that combines the infrared seeking of the Stinger missile with the warhead, rocket motor, and fuse from the Sidewinder missile for ASCM defense [4]. The typical configuration found on ships is the MK 49 launcher system, which has 21 missiles in cells ready to launch. The system receives input from the ship's fire control system. Once the target information is received, the launcher will line up at the appropriate direction and elevation and fire a missile. The missile uses an RF seeker to acquire the target, and when sufficient IR signal is received from the target, shifts to IR mode for the terminal phase of flight. The missile is able to rapidly maneuver (up to a maximum acceleration of 20 g's) to counter evasive measures by the incoming target.

The RAM has a high success rate against ASCM's, but it is not 100%. Time of flight to intercept a target allows range to close rapidly. If a RAM fails to kill the target, there will be little time to get the next RAM launched and the target will close to a short range, endangering the ship. Therefore, a preferred tactic is to fire two RAM at an incoming target to increase kill probability, utilizing the shoot-shoot-look method rather than the shoot-look-shoot method. This strategy gives a better probability of missile kill, but causes a rapid depletion of available weapons munitions and is expensive. The RAM system offers a greater engagement range and a higher hit probability than the CIWS.

Both systems are often used together such that the RAM provides longer range coverage and CIWS is used for short range defense against any missiles that get past RAM.

### 3. Airborne Laser System (ABL)

The ABL is an example of a directed energy weapon being designed to defend our forces against theater ballistic missile attacks. The ABL will engage a ballistic missile during the initial boost phase of flight and destroy the missile directly over, or near the launch site. The system consists of a megawatt class chemical oxygen iodine laser (COIL), beam control, transport section, and beam director. The system is mounted on a modified 747-400F aircraft with the beam director located in the nose cone section.

The COIL is a continuous beam laser that operates by injecting chlorine gas into a reservoir of hydrogen peroxide liquid to excite oxygen. Iodine gas is then injected into the excited oxygen to produce excited iodine that decays to its ground state by emitting a photon of wavelength 1.315 μm [17]. The photons are amplified in the lasing cavity and the energy is delivered through the beam transport system to the beam director. The beam director contains adaptive optics that use piezoelectric actuators that adjust the beam shape to minimize the affects of atmospheric distortion. The platform will operate around 45,000 feet to help minimize the atmospheric absorption and turbulence, to give the ABL an effective range of over 400 km [18].

The ABL system is evolving rapidly, and significant advances in laser technology have reduced the weight of the laser from 5500 lbs to just over 3000 lbs [4], not including the weight of beam control, beam director, or tracking systems. The program currently has one modified 747-400F that has the turret nose cone installed, with laser installation in progress. An expected operational test of the ABL is scheduled for sometime late in 2003, with an engagement of a Scud-like missile [17].

Advances in technology do not come cheaply. The estimated total program cost for the ABL, to include the first two aircraft, is over six billion dollars with each additional aircraft costing in excess of $500 million [18]. In addition to the system cost, the ABL has an estimated cost per engagement in the range of several thousand dollars a shot. The ABL does have limitations on the amount of chemical fuel that can be carried

but current estimates are that the system will be capable of firing the weapon a minimum of 20 times, with that number likely to grow in the future.

This program shows that directed energy weapons are becoming a reality. There are several weapons systems in various stages of development. Some other examples are the tactical high energy laser (THEL), and mid-infrared advanced chemical laser (MIRACL). High energy laser (HEL) weapons are likely to become a key component in combat systems over the next few decades. These new weapons provide speed of light capability with reduced time to kill and confirm that a target is destroyed. The ability to engage and kill anti-ship missiles at a greater range than current systems is a realistic goal with the use of a directed energy weapons. Directed energy weapons will provide greater protection for the ship, and eliminate collateral damage to the ship from missile debris striking the ship. One type of directed energy weapon being considered for missile defense is the free electron laser (FEL).

## B. BASIC DESCRIPTION OF A FREE ELECTRON LASER (FEL)

### 1. History of the Free Electron Laser

The concept for the free electron laser was first introduced by John Madey in 1971 [6], and in 1976 he demonstrated the first successful experiment using an FEL amplifier [7]. Interest in development of the FEL increased rapidly and by the 1980's research was heavily funded by the Strategic Defense Initiative. Development of FEL designs and technology have continued to the point where high power FEL's are now being considered for weapons applications again, including anti ship missile defense. Thomas Jefferson National Accelerator Facility (TJNAF) in Newport, Virginia has an operational FEL that has demonstrated an average power output of over 1kW and is currently being upgraded to 10 kW. Future plans include modifying the laser to achieve an average output power of 100 kW with a projected demonstration in 2005 [9]. The technology for the FEL has advanced rapidly to the point where a shipboard FEL missile defense system is possible within the next decade.

### 2. Electron Laser Basic Description

The free electron laser operates by passing a relativistic electron beam through an undulator that produces a periodic magnetic field developed by a series of opposing

magnets. The spatially oscillating magnetic field causes the electrons to follow sinusoidal trajectories. The acceleration of the electrons in the transverse direction causes them to emit radiation along the axis of the undulator. The light is contained between two mirrors that make up the optical resonator cavity. One mirror is partially transmissive to allow for light to escape the optical cavity and be used for the designed application of the laser. Figure 5 shows a basic FEL cavity.

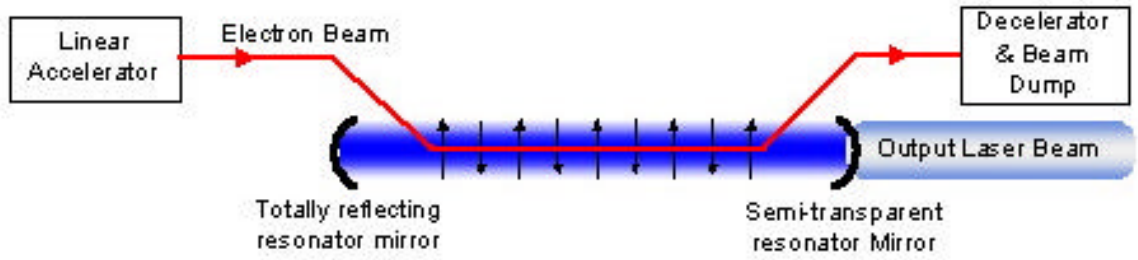


Figure 5. Oscillator FEL Cavity

As the light is reflected between the mirrors, it sets up an optical mode that is traveling in the same direction as the electron beam. The electron beam is not a continuous beam, but rather a series of pulses separated by a specific distance. This separation allows an electron pulse to enter the undulator in synchronism with the reflecting light pulse. As the electron pulse travels through the undulator in the presence of the light pulse, the electric field of the light interacts with the electrons, causing stimulated emission of more light. Over many passes, this creates a coherent light beam that continues to grow as the light reflects between the mirrors and interacts with more electron bunches. As the light intensifies in the cavity, saturation is reached where the output of the light is equal to the light created in the cavity.

The undulator and optical resonator cavity are where the laser beam is produced, but they are only a small part of the system that makes up the complete FEL system. Figure 6 shows a typical FEL system in a ring configuration with energy recovery.

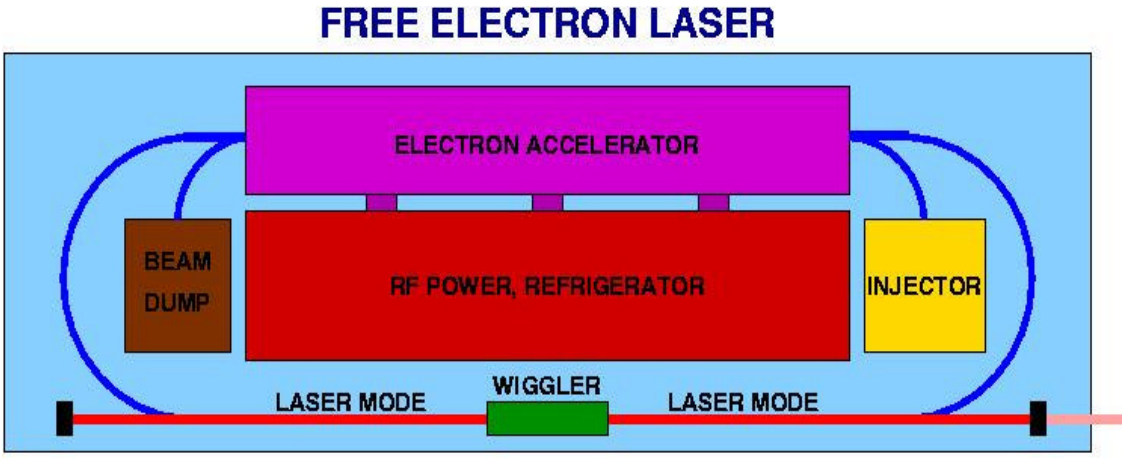


Figure 6. FEL Ring Configuration with Energy Recovery

The electron beam path is shown in blue, except where it overlaps the laser beam path shown in red. The electrons are generated in the injector by photoemission or thermionic emission, depending on the type of injector used, and accelerated to approximately 10 MeV by a strong electric field set up at the photo injector gun. The electrons are produced in a series of short pulses, typically on the order of millimeters in length, at a pulse frequency that is typically in the 100's of MHz range. The electron pulse leaves the injector and enters the linear accelerator where several hundred MeV of electron energy is gained. The accelerator uses radio frequency (RF) cavities to produce large electric fields that accelerate the electrons to their final energy, which can be as large as several hundred MeV. The electron beam is then directed into the undulator by a series of bending magnets. Inside the undulator, a few percent of the energy in the electron beam is converted into radiated energy in the form of laser light. The electron beam then leaves the undulator and is directed back into the linear accelerator. The electron beam enters the accelerator 180 degrees out of phase with the RF field in the accelerator and gives a large portion of its energy back to the cavity while the beam is decelerated by the RF field. The low energy electron beam exits the accelerator and is then directed to the beam dump, where the remaining energy of the electrons is dissipated.

This energy recovery technique has two positive affects on the system. First, it increases the overall efficiency by regaining energy from the electrons before dumping them. Second, it reduces the electron energy to less than 10 MeV, which is lower than the energy required for neutron generation; this prevents neutron irradiation from causing activation of materials in the beam dump and minimizes shielding requirements.

### 3. Other FEL Configurations

The proposed FEL for shipboard defense is an oscillator configuration with energy recovery. There are several other types of FEL configurations that may be used for other applications. The linear oscillator FEL with energy recovery, shown in Figure 7, removes the need for bending magnets. To accomplish energy recovery, a second linear accelerator and beam injector are used to inject electrons in the opposite direction of the first accelerator. The linear accelerators are positioned such that electrons coming out of the undulator are 180 degrees out of phase and give up energy into the rf cavities. With two opposing accelerators, the light beam is amplified in both directions due to the interaction with electron bunches from both accelerators. The additional space required for a second linear accelerator make this configuration impractical for shipboard application.

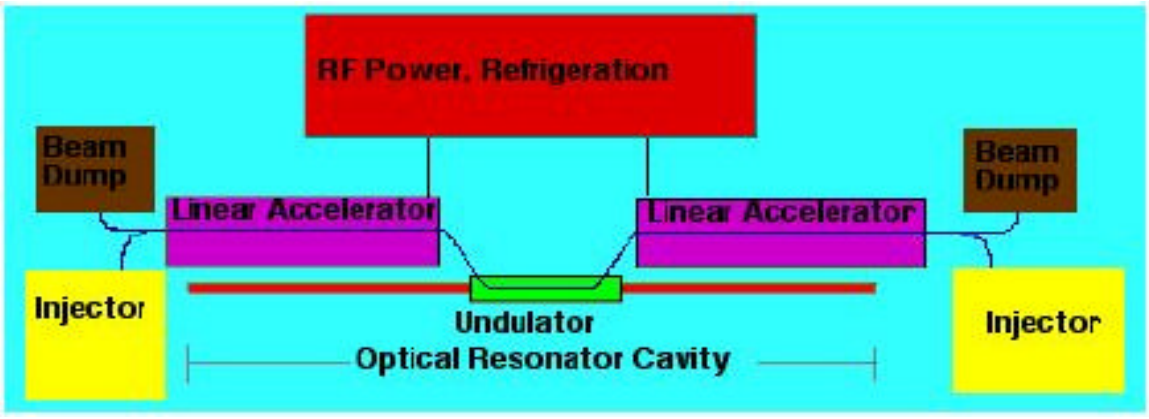


Figure 7. FEL Linear Configuration with Energy Recovery

Figure 8 shows an amplifier FEL configuration that is a single pass high gain design which extracts as much energy from the electron as possible during the pass. The disadvantage with the amplifier design is that due to electron beam dispersion from large energy removal, energy recovery is not possible. The higher energy electrons create

higher radiation levels at the beam dump and will have sufficient energy to cause neutron production and subsequent irradiation of material in the beam dump.

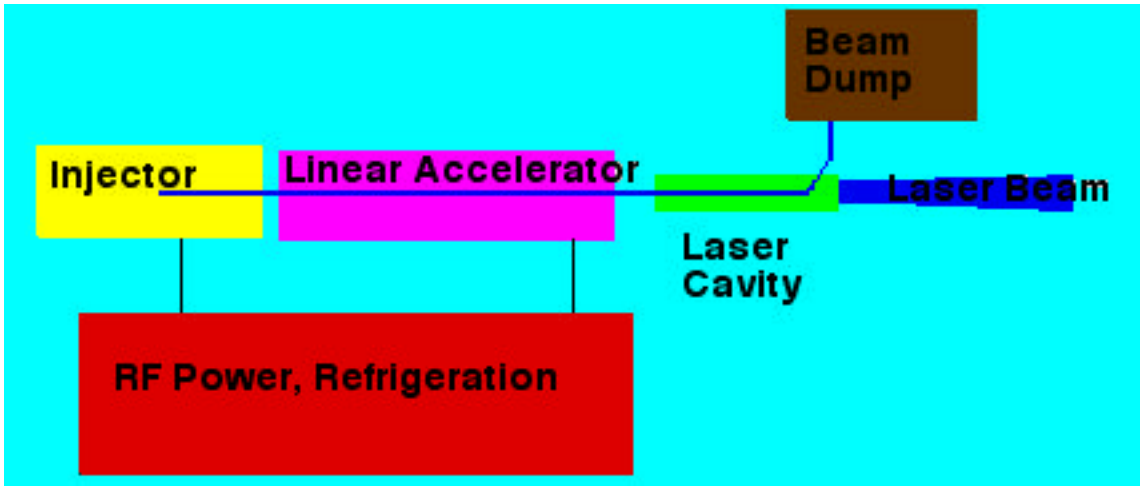


Figure 8. FEL Amplifier Configuration

In addition to the configurations discussed above, there are many other possible designs. Similar systems without energy recovery are common, but advances in technology have made energy recovery more attractive based on the increased efficiency of the system.

## C. FEL FOR MISSILE DEFENSE

The current missile defense systems aboard Navy ships are rapidly falling behind the developments in stealth and speed of anti-ship cruise missile technology. A high energy laser (HEL) system, such as a FEL, would be a positive asset for many reasons. The delivery of energy at the speed of light to a target reduces the range that an incoming threat missile can close on a ship before being destroyed. Figure 1 showed that the farther away a missile is destroyed, the less probable it is that a missile fragment will strike the ship. In addition to reduction in time of flight to the target, a HEL system allows for instant verification of a target kill and then allows for rapid reassignment to a different target if necessary. There are many types of HEL systems that are currently being developed for applications in the battles spaces of the future, but the FEL offers

many advantages for shipboard applications that other HEL systems are not capable of matching. The FEL also offers advantages over conventional type weapons such as RAM, and CIWS.

### 1. Advantages of the FEL

#### *a. Supply*

Future plans for all-electric drive ships will make large amounts of electrical power available for weapons application. With this electrical energy available for use by the weapons system, a high power FEL would be able to operate and engage targets for as long as the ship's electrical system can supply power. Conventional anti-ship missile defense systems that rely on an inventory of missiles or ammunition, and chemical laser systems that require a chemical source, face the problem of running out of the required munitions and require an out of service period for reloading. The FEL would be never have to be removed from service to undergo reloading operations, making it much more reliable.

#### *b. Tunable Wavelength*

The FEL operating wavelength is tunable, which gives the ability to exploit wavelength-dependent atmospheric propagation windows. By minimizing atmospheric absorption, the effective range is increased and the time required to damage a target is decreased. Other types of lasers such as the chemical laser, eximer lasers, and solid state lasers can only operate at only one specific wavelength. One example of a non-tunable laser is the MIRACL system, a deuterium-fluoride laser that operates at 3.8 μm [8]. The wavelength ($l$) is determined by the energy levels excited in the chemical reactions of the lasing process making it impossible to change the wavelength of the laser to minimize atmospheric absorption.

#### *c. Reliability*

The FEL design requires a minimum amount of maintenance since there are no moving parts. The components are all electrical, with the exception of some support equipment such as the refrigeration/cooling units and the beam director. The FEL at TJNAF is currently undergoing an upgrade to 10 kW and is projected to have 10,000 hours of continuous operation before a scheduled maintenance period. This type

of reliability will be a great improvement over current existing systems that require more frequent periodic maintenance and repairs. The Phalanx CIWS is, on average, only available 76 % of the time for a variety of reasons that include hydraulic problems, lack of onboard repair and preventive maintenance parts, and overhauls [5]. In addition to system reliability, the FEL offers another distinct advantage over missile systems. A beam of light has very little chance of suffering a catastrophic failure before getting to its designated target, but a missile has many failure mechanisms that may prevent it from reaching the target. The FEL, with minimal maintenance requirements and high reliability, will greatly improve anti-ship missile defense capabilities.

***d. Exhaust***

The FEL converts energy from an electron beam into a high energy light beam without the use of a chemical fuel. There are no noxious gases or plumes that must be vented off ship, unlike a chemical laser or missile system. This minimizes controls for hazardous materials and eliminates the need for expensive clean up in areas that are exposed to hazardous chemicals.

***e. Mission Flexibility***

The FEL is an adaptable weapons system capable of taking on many roles. Unlike other defensive weapons systems like the CIWS and RAM that are specifically designed only for missile defense, the FEL would be capable of defending against many other threats such as small ships, aircraft, and jet ski's. In addition to a defensive role, the FEL can also be used for precision strike capability in littoral waters. The ability to target and destroy key equipment and assets with no collateral damage make the FEL an attractive alternative to a missile strike. The precision strike capability would naturally be limited to line of sight targets that are located close to the coastline so that they would be within the range of the FEL. But there are now studies that consider using relay mirrors to re-direct the laser beam to the battlefield

***f. Operating Cost***

The cost per engagement for a FEL is much less than that of other weapons systems. The only cost incurred for firing the weapon is the cost of the fuel required to generate the energy used by the FEL, less than $2.00. In comparison, the cost

of one RIM-116A Rolling Airframe Missile (RAM) is $273,000 and one RAM is $444,000 [4]. A detailed cost analysis for the FEL is presented in section C. 3. of this chapter.

### 2. Disadvantages of the FEL

The FEL has many advantages as a weapons system, but there are also some disadvantages compared to other weapons systems. The first disadvantage is the high initial cost for the system, crudely estimated around $50 million. Cost analysis for the FEL is presented in section 3.

The other disadvantages of the FEL are related to beam propagation through the atmosphere. As mentioned in the advantages section, the atmosphere absorbs energy as the light beam travels through it. Although the FEL's ability to tune the wavelength can minimize atmospheric absorption, it can't eliminate it. Atmospheric absorption can change drastically based on environmental conditions. Fog, raindrops, and suspended aerosols cause additional scattering and absorption. As the particle density increases, the amount of absorption and scattering increase, resulting in a much lower beam intensity at the target. Fog, rain, dust, smoke, and other suspended aerosols greatly reduce the effective range of the FEL and may reduce intensity to the point that the weapon may be ineffective. Fortunately, these same adverse conditions affect the sensors on the threat missile.

Another beam related disadvantage is thermal blooming, which occurs when a section of the atmosphere absorbs a small amount of energy and begins to slightly increase in temperature. The refractive index of air is a function of temperature, and as the temperature changes in the center of the column of air being heated by the laser beam, it begins to act as a diverging lens and causes the beam to diverge. This problem is made worse with higher atmospheric absorption and beam intensities. Thermal blooming models use a critical blooming time, $t_c$ , that estimates the time it takes for a column of air to be heated to the point that thermal blooming occurs. By ensuring that the beam does not heat a section of air for longer than the critical blooming time, thermal blooming can be avoided. Cross winds and slewing rate of the beam help to prevent thermal

blooming by changing out the volume of air in the beam. This is known as channel clearing. Thermal blooming will be discussed in more depth in a later chapter.

### 3. Cost Comparison of the FEL vs Other ASCM Defense Systems

A cost analysis of the FEL against current ASCM defense systems shows that the FEL system is a feasible alternative that may offer long term cost savings. The cost analysis is broken into two different areas: initial weapon cost and cost per engagement.

Initial cost of the RAM system is $17.2M and includes $7.9M for the launcher and $9.3M for 21 missiles at $444,000 each [3b.][4]. This cost only provides for one launcher on the ship and does not provide for any additional missiles other than those loaded into the launcher. The initial cost for the Phalanx CIWS is $3.8M and includes the cost for one mount and 5000 rounds of ammunition [3a.]. The current estimate of a MW class FEL is $55 million [9]. While the initial cost is significantly more than the initial cost of the Phalanx or RAM systems, once the FEL is installed, there are no additional costs for ammunition, missiles, or stockpile and storage of these munitions.

Cost per engagement is based on a single engagement of an ASCM. Based on weapons doctrine, the normal tactic is to launch 2 RAM at an incoming threat missile. Total cost for two RAM is $888,000. For the CIWS, an average of three (3) seconds firing time is assumed to kill the incoming threat missile, which equates to 225 rounds of ammunition. Total cost for 225 rounds is $13,500 [3a.]. The FEL requires approximately five seconds lasing time to put required energy on target to destroy it. For a FEL efficiency of 10%, this requires 50 MJ of energy from the ships electrical system. One gallon of fuel contains 113.5 MJ of energy. Take as an example, an LM2500 turbine which converts fuel to mechanical energy at a rate of 0.435 lbs fuel/HP-HR. For a generator with a 90 % conversion efficiency from mechanical to electrical power, one pound of fuel will yield 5.54 MJ of energy. To get the required 50 MJ of energy for the FEL, 9 lb, or 1.2 gallons of fuel are consumed. Using an average price of $1.40 per gallon, the total cost per engagement for the FEL is only $1.68. This low cost per engagement gives the ability to use the weapon for live fire testing and training at low costs. The other two systems are rarely used for training due to large operating costs, so personnel training is accomplished by simulations or walk through of procedures. Based

on the low operational cost for the FEL, savings over decades of use make the system cost effective and in line with other weapons systems. Table 1 shows a summary of the cost comparison for the FEL, RAM and CIWS.

| | **FEL** | **RAM** | **CIWS** |
|---|---|---|---|
| **Unit Cost** | $55M | Launcher - $7.9M<br>Missiles - $9.3M<br>Total - $17.2M | Mount - $3.2M<br>Ammo (10,000) - $0.6M<br>Total - $3.8M |
| **Cost per engagement** | 2 Seconds fuel<br>$1.68 | 2 Missiles<br>$888,000 | 225 rounds<br>$13,500 |

Table 1. Cost Analysis Summary

Although the FEL is more expensive than RAM and CIWS for initial installation, over the lifetime of the weapon system, the FEL's low cost per engagement coupled with the advantages listed above make the FEL a valuable asset that will greatly improve protection for ships against ASCM's.

A system lifetime total cost is presented in table 2 using an assumed 20 year life with an average of 10 launches per year.

| | **FEL** | **RAM** | **CIWS** |
|---|---|---|---|
| **Initial Cost**<br>**+**<br>**Ammunition Cost** | $55M<br>+<br>200 * $2.00=<br>$400 | $17.2M<br>+<br>200*$888,000=<br>$178M | $3.8M<br>+<br>200*$13500=<br>$2.7M |
| **Total Cost** | ≈ $55M | ≈$190M | ≈$6.5M |

Table 2. Lifetime Cost Analysis

THIS PAGE INTENTIONALLY LEFT BLANK

# III. DETAILED DESCRIPTION OF A FEL

The FEL at TJNAF is currently being upgraded to an average output of 10 kW. Additional modifications are expected to increase that power output to 100 kW by 2005. These rapid advances in design and technology make a FEL with an average power of 1 MW appear possible in the future. Simulations and modeling for the 100 kW FEL design at TJNAF are presented in this paper. Figure 9 is a diagram of the proposed 100 kW FEL system at TJNAF [14].

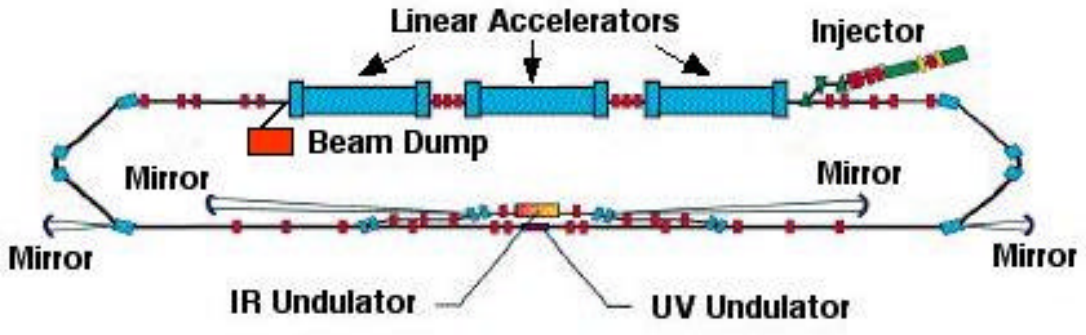


Figure 9. 100 kW FEL System Diagram (after [14])

There are two major subsystems to consider for the FEL: the electron beam control subsystem and the optical beam control subsystem. There are also additional auxiliary systems associated with the FEL such as refrigeration, cooling water, and shielding.

## A. ELECTRON BEAM CONTROL SUBSYSTEM

The electron beam control subsystem is composed of the injector, linear accelerators, beam dump, and beam transport subsystem. The electron life cycle can be traced in Figure 9. The electrons are generated in the injector, accelerated to high energies in the accelerator modules, pass through the undulator where they give up a small amount of their energy to create the coherent laser beam, pass back through the linear accelerators where they give up the majority of their energy, and are then dissipated in the beam dump.

## 1. Injector

The proposed injector design for the 100 kW FEL at TJNAF is a superconducting, 500 kV DC, photocathode electron gun with a GaAs cathode that is driven by a green laser [15]. Figure 10 is a cutaway view of the proposed injector.

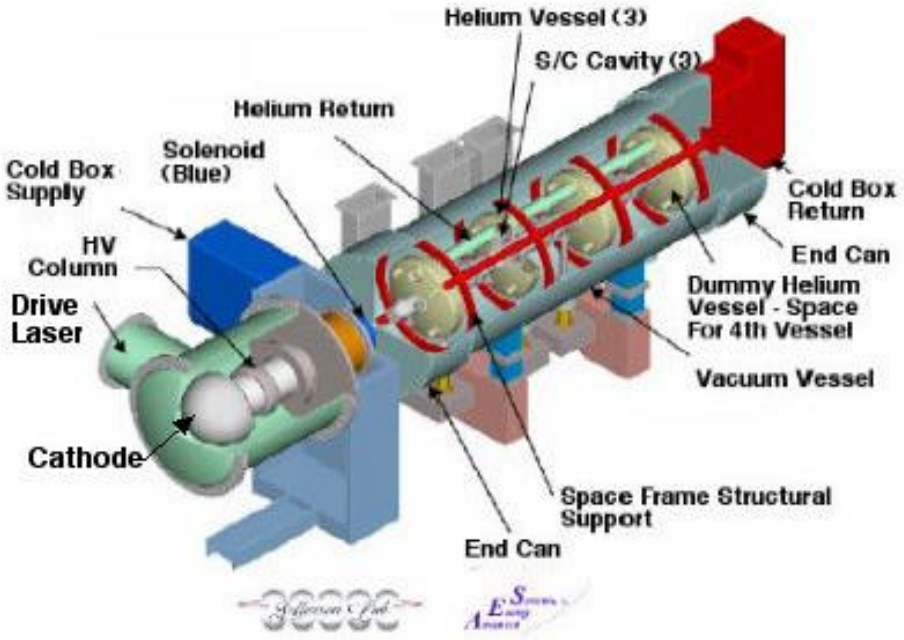


Figure 10. Injector Cutaway (after [15])

The injector generates the electrons in short periodic pulses by photoelectrically exciting the electrons off the cathode using a pulsed green laser. Once the electrons are removed from the cathode, they are rapidly accelerated by a strong electric field set up by the high voltage (HV) column. It is important to rapidly accelerate the beam as it exits the cathode to minimize space charge effects due to Coulomb forces. The space charge forces cause the electron beam quality to degrade by causing the beam to spread in the transverse and longitudinal directions. The beam leaves the HV column and enters a series of three accelerator cavities that raise the energy of the electrons to greater than 7 MeV before exiting the injector.

The gun is designed to operate with the following parameters to provide a high quality electron beam input to the superconducting RF (SRF) accelerators [12]:

| | | |
|---|---|---|
| Pulse Repetition Rate | $W$ | 750 Mhz |
| Peak Current | $I_{pk}$ | 270 A |
| DC Voltage | $V_{gun}$ | 500 kV |
| Electron Energy | $E_{inj}$ | > 7 MeV |
| Energy Spread | $DE$ | < 1.0 % rms |
| Transverse Emittance (normalized) | $e_n$ | < 3 π mm-mrad |
| Electron pulse Length | $l_e$ | 0.1mm |

## 2. Accelerator

After leaving the injector, the electron beam enters the linear accelerators and is accelerated to relativistic energies. At such high energy, the space charge forces become insignificant and can be neglected in later calculations. The electron beam enters the accelerator at energies of approximately 7 MeV and is accelerated to a final beam energy of 210 MeV. The electrons enter the accelerator in phase with the RF field and are accelerated as they pass through the cavities. After leaving the accelerator the beam is directed to the undulator, where it gives up a small amount of its energy to the optical beam. After passing through the undulator, the electrons are returned to the accelerator 180 degrees out of phase with the RF field, causing the electrons to decelerate by giving energy back to the RF field.

The design parameters for the SRF accelerators are:

| | | |
|---|---|---|
| Pulse Repetition Rate | $W$ | 750 MHz |
| Acceleration Gradient | $(DE/L)_{acc}$ | 20 MeV/m |
| Number of Modules | | 3 |
| Output Energy | $E_b$ | 210MeV |
| Accelerator Efficiency | $h_{rf}$ | 60% |

## 3. Beam Dump

The decelerated electron beam leaves the accelerators with less than 10 MeV of energy and enters the beam dump where the electrons and their energy are dissipated. By recovering the electron beam energy, the overall efficiency of the FEL is greatly increased. Due to degradation of beam quality, the electron beam can not be used for more than one pass through the undulator.

The beam dump consists of a block of metal into which the electron beam is dissipated, and a cooling system that removes the generated heat from the metal to a heat sink. Radiation shielding of the beam dump is required due to the production of gamma rays from Bremsstrahlung (braking radiation) produced as the energy of the electron beam is dissipated [13]. One advantage of the energy recovery system is that the final energy of the electron beam has been reduced below the energy required for neutron generation. The low energy gammas require less shielding than would be required for neutrons, which would activate adjacent materials and create additional radiation.

#### 4. Beam Transport Subsystem

The beam transport system consists of piping and bending magnets. The electron beam must be contained in high vacuum ($10^{-11}$ Torr) to prevent interaction with gas particles. The beam is guided by a series of bending magnets that force the electron beam to change directions due to field interactions. The acceleration of the electrons due to these directional changes causes synchrotron radiation projected into a narrow forward radiation cone much like a flashlight [13].

### B. LIGHT BEAM CONTROL SUBSYSTEM

Laser light from the FEL is transported to a beam director on the deck of the ship that sends the beam to the intended target. The major components of the light beam control subsystem are the undulator, optical resonator cavity , and transport subsystem.

#### 1. Undulator

The undulator, also called the wiggler, is contained in the optical cavity and is the heart of the FEL. Figure 11 shows a detailed drawing of the optical resonator cavity and undulator [16].

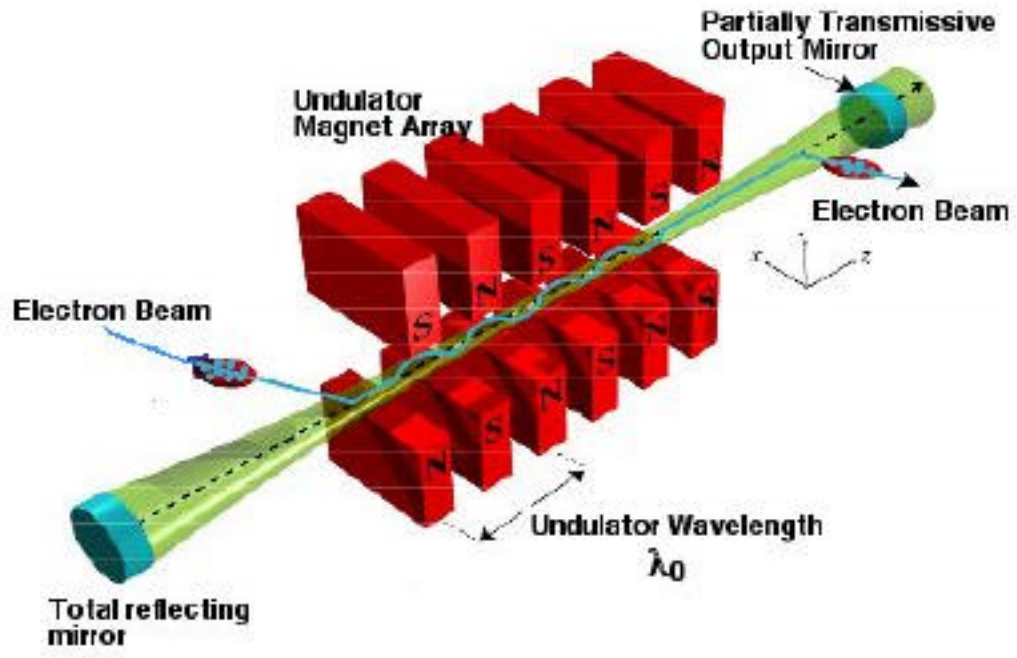


Figure 11. Optical Resonator Cavity and Undulator of FEL (after [16])

The electron beam is directed into the undulator where an oscillating magnetic field is set up using a series of alternating permanent magnets. The parameters of the undulator are:

| | | |
|---|---|---|
| Undulator Length | $L$ | 2.88 m |
| Undulator Wavelength | $l_0$ | 0.08 m |
| Number of Undulator Periods | $N$ | 36 |
| Undulator Parameter | $K$ | 1.7 |

## 2. Optical Resonator Cavity

The optical resonator cavity is comprised of two mirrors that are spaced a distance apart so that the reflecting optical pulses interact in phase with the sequence of pulses from the electron beam. As the electron pulses travel through the undulator in the presence of a light pulse, stimulated emission of light occurs. The resulting coherent laser beam continues to be amplified by each successive electron pulse passing through the undulator.

The mirrors are a key component in the FEL design and must be capable of withstanding high power densities. Based on an optical coupling output of 20 %, the power incident on the mirrors will be 500 kW to generate the 100 kW output. Power

density at the mirrors is well within limits for this power, but could become a factor when increasing power output of the laser. Use of short Rayleigh lengths to increase mirror spot size, and therefore minimize power densities at the mirrors, is discussed in section V. One of the mirrors is partially transmissive to allow a percentage the light beam to escape and become the output of the laser. The length of the optical resonator cavity ($S$) is 32 m.

### 3. Optical Transport Subsystem

The optical transport subsystem is similar to the beam transport subsystem. It consists of pipes and mirrors that transport the light beam from the FEL to the beam director for use. In a weapon system, the light beam will be guided to a beam director that will aim and send the light beam to the intended target.

## C. AUXILIARY SYSTEMS

The FEL requires several support systems and an adequate power supply for continuous operation. Some of the required systems are the refrigeration system, fresh water cooling, shielding, and power supply. A brief description and purpose of each system follows.

### 1. Refrigeration System

The refrigeration system is required to provide liquid helium to the injector and accelerator. Cooling of the accelerator cavities to 2 K is required to eliminate resistance losses that would occur in the cavity walls with such high electric fields. Supercooling the cavities makes them superconducting, thereby eliminating $I^2$ R losses.

### 2. Fresh Water Cooling System

The fresh water cooling system is required to remove excess heat generated in the beam dump. The energy deposited in the beam dump must be removed to prevent overheating and damage to the beam dump.

### 3. Shielding

Operation of the FEL presents a radiation hazard that requires sheilding. Bremsstrahlung radiation is generated in the beam dump and synchrotron radiation is generated in the areas where the electron beam direction is changed. The gamma rays

generated during FEL operation must be shielded to minimize radiation levels in the general area.

### 4. Vibration Control

Vibrations due to coupling with external sources can cause mirror vibrations and motion of precisely aligned equipment. To reduce the effects on the system, vibration isolation mounting is used. The FEL resonator mirrors require very precise alignment and must be maintained within a few microns for proper FEL operation. An active mirror alignment system is required to maintain alignment of the laser cavity and optical transport mirrors.

THIS PAGE INTENTIONALLY LEFT BLANK

# IV. FEL THEORY

The free electron laser uses a relativistic electron beam, an undulator, and an optical resonator cavity to produce a high power, coherent, laser beam. Early theoretical descriptions of the FEL utilized quantum electrodynamics, but the development of a classical approach later proved to be both accurate and easy to understand [19]. The classical FEL theory will be described in the following sections.

## A. RESONANCE

In order for an FEL to have gain, a net transfer of energy from the electron beam to the optical wave must occur. The optimum energy exchange between an optical field and electron occurs when one wavelength of light passes the electron in one undulator period. This is called the "resonance condition" and can be demonstrated as a race down the undulator between a photon and an electron where the photon wins the race by one optical wavelength. Figure 12 shows a diagram of the electron-photon race [21]. The optical wavelength $l$ is shown in blue, the electron is red, and the undulator wavelength $l_0$ is in green.

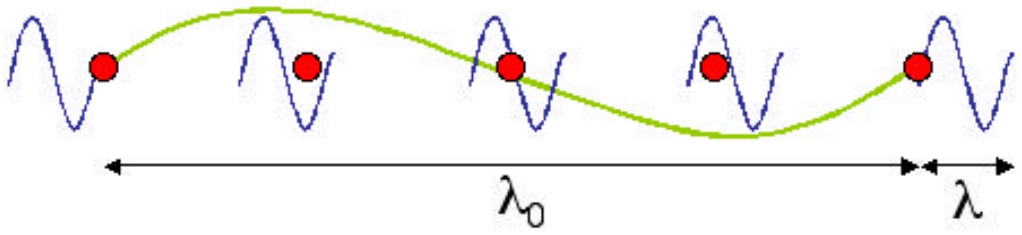


Figure 12. Electron – Photon Race

The relationship between the undulator wavelength and the optical wavelength can be developed from the resonance condition. For a given reference electron, a wavelength of light will travel a distance $l$ ahead of the electron over one undulator period. Take $Dt$ to be the time it takes an electron to travel through one undulator wavelength $l_0$ at speed $v_z$. This is equal to the time required for the photon to go a distance $l_0 + l$ at the speed of light $c$, so that

$$\Delta t = \frac{l_0}{v_z} = \frac{l_0 + l}{c}. \tag{4.1}$$

Solving for $l$ with $b_z = v_z/c$ gives the resonance condition,

$$l = \left(\frac{1 - b_z}{b_z}\right) l_0 . \tag{4.2}$$

The Lorentz factor is

$$g = \frac{1}{\sqrt{1 - b_z^2 - b_\perp^2}} = \frac{1}{\sqrt{1 - b_z^2 - K^2/g^2}} \tag{4.3}$$

where $K = e\ B_u\ l_0 /(2\ \pi\ m_e\ c^2)$ is the dimensionless undulator parameter and $b_\perp = K/g$. (to be derived later in the electron dynamics section). Inserting $K/g$ for $b_\wedge$ into equation 4.3 and solving for $b_z$ we get

$$b_z = \sqrt{1 - \frac{1 + K^2}{g^2}} \approx 1 - \frac{1 + K^2}{2g^2}. \tag{4.4}$$

The last approximation is made using the binomial expansion since $K$ is of order unity and $g^2 >> 1$. Inserting equation 4.4 into equation 4.2, the optical wavelength becomes

$$l = \frac{\left(1 - 1 + \left[\frac{1 + K^2}{2g^2}\right]\right)}{\left(1 - \left[\frac{1 + K^2}{2g^2}\right]\right)} l_0 . \tag{4.5}$$

Since $1 + K^2/2g^2 << 1$, the denominator is ≈ 1 and the resonance condition can be written as

$$l = \left(\frac{1 + K^2}{2g^2}\right) l_0 . \tag{4.6}$$

Equation 4.6 demonstrates that for a given undulator, the wavelength of light becomes a function of the electron energy $E_e = g\,mc^2$ and the undulator magnetic field $B_u$ through $K$.

## B. ELECTRON MOTION

### 1. Spontaneous Emission

The electron trajectories in the undulator determine the character of FEL interactions [19]. Initially, there is no optical field in the resonator cavity; it is created by spontaneous emission from the electrons traveling through the undulator. Spontaneous emission of the electron occurs when the electron is accelerated - in this case the electrons oscillate transversely due to interaction with the magnetic field of the undulator. The power radiated by the relativistic electron, $P_e$ , is given by the relativistic Larmor formula [21]:

$$P_e = \frac{2\,e^2\,g^4\,\dot{b}_\perp^2}{3\,c} \tag{4.7}$$

where $\dot{b}_\perp = Kk_0c/g$ is the transverse acceleration, $k_0 = 2\pi/l_0$, and $\underline{e}$ is the charge of an electron [20]. The photons emitted by the electron will have an energy $E = hc/l$ where $h$ is Planck's constant. By using the resonance condition for $l$, $k_0 = 2\pi/l_0$ , and equation 4.7, the energy of the emitted photon can be written as

$$E_{ph} = \frac{2\,\hbar\,c\,k_0\,g^2}{1+K^2}. \tag{4.8}$$

The number of photons emitted spontaneously by one electron in one pass through the undulator, $W_e$ , can be determined from the power emitted by the electron, the energy per photon emitted, and the total time the photon is in the undulator

$$W_e = \frac{P_e \Delta t}{E} \tag{4.9}$$

$$W_e = \frac{2\,p\,N\,a\,K^2\,(1+K^2)}{3} \tag{4.10}$$

where $a = e^2/\hbar c \approx 1/137$, is the fine structure constant. For a typical FEL with N≈$10^2$ and K≈1, an electron emits approximately one photon per pass in the undulator into a narrow forward cone of solid angle $g^2$. However, not all of the photons are emitted into the coherent optical mode. Only a small percentage of the photons emitted into the $g^2$ cone are within the smaller solid angle, $1/Ng^2$ determined by the coherent optical mode [19]. The number of photons emitted into the coherent optical mode during one pass through the undulator is then

$$W_c \approx a\ K^2\left(1+K^2\right)\ . \tag{4.11}$$

The total photon energy emitted by the electron is many orders of magnitude less than the total energy of the electron, therefore, the momentum recoil has a negligible effect on the electron's path. The process of spontaneous emission from the electrons will not generate large power outputs, but it is necessary for the start-up mechanism in the FEL. In a typical FEL, the number of electrons in a pulse is on the order of $10^{10}$. The number of photons emitted into the coherent optical mode during the first pulse through the undulator is sufficient to establish a classical optical field that is amplified through stimulated emission of subsequent electron pulses.

### 2. Electron Dynamics – the Pendulum Equation

Now that an optical field has been developed in the FEL, the interactions of the electrons with the alternating static magnetic field of the undulator, $\vec{B}_u$, and the moving electric and magnetic fields of the optical wave, $\vec{B}_s$ and $\vec{E}_s$, can be analyzed. The fields for a helical undulator can be written as [21]:

$$\vec{B}_u = B_u\ \left(\cos(k_0\ z), \sin(k_0\ z), 0\right) \tag{4.12}$$

$$\vec{B}_s = E_s\ \left(\sin(\Psi),\ \cos(\Psi),\ 0\right) \tag{4.13}$$

$$\vec{E}_s = E_s\ \left(\cos(\Psi),\ -\sin(\Psi),\ 0\right) \tag{4.14}$$

in cgs units where $\Psi = (kz-wt+f)$ is the phase of the optical wave, $k = w/c$ is the optical wave number, and $f$ is the initial optical phase at $t = 0$ and $z = 0$.

The forces acting on the electrons are given by the Lorentz force equation, and the equation for the change in electron energy $E_e$ ,

$$\vec{F} = \frac{d\vec{p}}{dt} = -e\left(\vec{E_s} + \vec{b}\times\vec{B}\right) \tag{4.15}$$

$$\frac{dE_e}{dt} = -e\ \vec{v}\cdot\vec{E_s}\,. \tag{4.16}$$

Using the relations, $\vec{p} = g\ m_e\vec{v} = \vec{b}\ g\ m_e c$, and $E_e = g\ m_e c^2$, equations 4.15 and 4.16 can be rewritten,

$$\frac{d(g\,\vec{b})}{dt} = -\frac{e}{m_e\ c}\left(\vec{E_s} + \vec{b}\times\vec{B}\right) \tag{4.17}$$

$$\frac{dg}{dt} = -\frac{e}{m_e\ c}\ \vec{b}\cdot\vec{E_s}\,. \tag{4.18}$$

Substituting the fields into equation 4.17, the transverse components can be written as

$$\frac{d(g\,\vec{b_x})}{dt} = -\frac{e}{m_e\ c}\left(\vec{E}_{sx} + \vec{b}_z\times\vec{B}_{uy} + \vec{b}_z\times\vec{B}_{sy}\right)$$

$$\frac{d(g\,\vec{b_x})}{dt} = -\frac{e}{m_e\ c}\left(E_s(1-b_z)\cos(\Psi) - B_u b_z \sin(k_0\ z)\right) \tag{4.19}$$

and

$$\frac{d(g\,\vec{b_y})}{dt} = -\frac{e}{m_e\ c}\left(\vec{E}_{sy} + \vec{b}_z\times\vec{B}_{ux} + \vec{b}_z\times\vec{B}_{sx}\right)$$

$$\frac{d(g\,\vec{b_y})}{dt} = -\frac{e}{m_e\ c}\left(-E_s(1-b_z)\sin(\Psi) + B_u b_z\cos(k_0\ z)\right). \tag{4.20}$$

For relativistic electrons, 1- $b_z$ <<1, equations 4.19 and 4.20 can be simplified, and written together as $\frac{d(g\,\vec{b}_\perp)}{dt} = \frac{-e\ B_u\ b_z}{m_e\ c}(-\sin(k_0\ z),\ \cos(k_0\ z),\ 0)$ . (4.21)

Integrating equation 4.21 gives (assuming constants of integration are zero for perfect injection into the helical orbits)

$$\vec{b}_{\perp} = \frac{-e\ B_u\ l_0}{g\ m_e\ c^2\ 2\ p}(\cos(k_0\ z), \sin(k_0\ z), 0). \tag{4.22}$$

Defining the dimensionless undulator parameter as $K = e\ B_u\ l_0 /(2\ \pi\ m_e\ c^2)$, equation 4.22 becomes

$$\vec{b}_{\perp} = \frac{-K}{g}(\cos(k_0\ z), \sin(k_0\ z), 0). \tag{4.23}$$

The transverse motion of electrons in the helical undulator is described by equation 4.23.

Substituting the electric field from equation 4.14 into equation 4.18, the second Lorentz equation becomes

$$\frac{dg}{dt} = -\frac{e}{m_e\ c}\ \left(b_x, b_y, b_z\right) \cdot E_s\left(\cos\Psi, -\sin\Psi, 0\right). \tag{4.24}$$

Inserting equation 4.23 for $\vec{b}_{\perp}$ into equation 4.24 and using the trigonometric identity $\cos(a+b)=\cos(a)\cos(b) - \sin(a)\sin(b)$, equation 4.24 becomes

$$\frac{dg}{dt} = \frac{e\ K\ E_s}{g\ m_e\ c}\ \cos(k_0\ z + \Psi)$$

$$\frac{dg}{dt} = \dot{g} = \frac{e\ K\ E_s}{g\ m_e\ c}\ \cos(z + f) \tag{4.25}$$

where $z = (k+k_0)\ z - w\ t$ is the electron phase.

By rearranging equation 4.4 and taking the time derivative, a relationship between $\dot{g}$ and $\dot{b}_z$ can be developed;

$$\frac{d}{dt}\left(g^{-2}(1-K^2) = 1 - b_z^2\right)$$

$$-2\ g^{-3}\ \dot{g}\ (1+K^2) = -2\ b_z\ \dot{b}_z$$

$$\frac{\dot{g}}{g} = \frac{g^2\ b_z\ \dot{b}_z}{\left(1+K^2\right)}. \tag{4.26}$$

Taking the first time derivative of the electron phase, $z$, we get

$$\dot{z} = (k + k_0)v_z - w = (k + k_0)c\beta_z - w\,, \tag{4.27}$$

and the second derivative is

$$\ddot{z} = (k + k_0)c\dot{\beta}_z\,. \tag{4.28}$$

Solving for $\dot{\beta}_z$ yields

$$\dot{\beta}_z = \frac{\ddot{z}}{(k + k_0)c}\,. \tag{4.29}$$

Substituting equation 4.29 into equation 4.26,

$$\frac{\dot{\gamma}}{\gamma} = \frac{\gamma^2 \beta_z \ddot{z}}{\left(1 + K^2\right)\left(k + k_0\right)c}\,. \tag{4.30}$$

Using the resonance condition (equation 4.6), $(k+k_0)c \approx kc = w$ since $k_0 << k$ for relativistic electrons, and solving for $\dot{\gamma}$, equation 4.30 becomes

$$\dot{\gamma} = \frac{\ddot{z}\,\gamma}{2\,w_0} \tag{4.31}$$

where $w_0 = k_0\,c = 2\pi/l_0$.

Equations 4.25 and 4.31 can be combined and solved for $\ddot{z}$

$$\dot{\gamma} = \frac{\ddot{z}\,\gamma}{2\,w_0} = \frac{e\,K\,E_s}{\gamma\,m_e\,c}\,\cos(z + f)$$

$$\ddot{z} = 2\,w_0 \frac{e\,K\,E_s}{\gamma^2\,m_e\,c}\,\cos(z + f)\,. \tag{4.32}$$

Equation 4.32 is the electron equation of motion and describes electron phase dynamics in the form of the pendulum equation. This equation can be written using the dimensionless time parameter $t = ct/L$, where $t$ is the time and the undulator length is $L$. In a single pass through the undulator, $t$ goes from 0 to 1. For clarity, derivatives with respect to dimensionless time will be indicated as $dX/dt = \mathring{X}$ and the second derivative

will be $\ddot{X}$, where $X$ can be any parameter. The pendulum equation can be rewritten as a second-order differential equation with respect to $t$ as

$$\ddot{z} = 2\, w_0 \frac{e\, K\, E_s}{g^2\, m_e\, c} \left( \frac{L^2}{c^2} \right) \cos(z + f), \tag{4.33}$$

where the $L^2/c^2$ term comes from the substitution of $d^2t=(L/c)^2\, d^2t$. The group of terms in front of the cosine can be written as one variable, defining the magnitude of the dimensionless optical field $a = |a|e^{if}$. After some simplifications, it can be shown that the field is

$$|a| = \frac{4p\, Ne\, K\, E_s L}{g^2\, m_e\, c^2}. \tag{4.34}$$

so that the pendulum equation can be rewritten as

$$\ddot{z} = \dot{v} = |a| \cos(z + f). \tag{4.35}$$

where the dimensionless electron phase velocity $v$ is equal to

$$v = \dot{z} = L\left[ (k + k_0)\, b_z - k \right]. \tag{4.36}$$

Equation 4.36 governs the phase-space motion of electrons traveling through the undulator interacting with an optical wave of magnitude $|a|$. The cosine term determines if the electron gains or loses energy to the optical field. The electrons with phases from $-p/2$ to $p/2$ gain energy from the optical field while, those with phases from $p/2$ to $3p/2$ transfer energy to the optical field. As the electrons in the pulse interact with the optical field, they bunch over the optical wavelength. The optical field strength determines the rate of electron bunching. For $|a| < \pi$, the field is weak and the bunching is small, while for $|a| > \pi$, the field is strong and bunching is strong.

## C. OPTICAL WAVE EQUATION

The pendulum equation describes how electron motion is affected by the presence of an optical field. This section will develop the equations to show how the optical field is affected by the electron beam. The wave equation that governs the propagation of the optical wave is

$$\left(\nabla^2 - \frac{1}{c^2}\frac{\partial^2}{\partial t^2}\right)\vec{A} = -\frac{4p}{c}\vec{J}_\perp \tag{4.37}$$

where $\vec{A}$ is the vector potential for a circularly polarized plane wave and $\vec{J}_\perp$ is the transverse current density. For a slowly varying amplitude and phase of the optical beam, the vector potential can be written as a function of *z* and *t*,

$$\vec{A}(z,t) = \frac{c}{w}E_s\left(\sin(\Psi),\cos(\Psi),0\right) \tag{4.38}$$

and

$$\vec{B}_s = \vec{\nabla}\times\vec{A}. \tag{4.39}$$

The transverse directions are neglected using the assumption that the electron beam radius is small compared to the optical mode. The spatial and time derivatives of 4.37 are

$$\frac{\partial^2\vec{A}}{\partial z^2} = \frac{2}{k}\frac{\partial E_s}{\partial z}\left(k+\frac{\partial f}{\partial z}\right)\left(\cos(\Psi),-\sin(\Psi),0\right) + \frac{1}{k}E_s\left(-\sin(\Psi),-\cos(\Psi),0\right)\left(k+\frac{\partial f}{\partial z}\right)^2 \tag{4.40}$$

and

$$\frac{\partial^2\vec{A}}{\partial t^2} = \frac{2}{k}\frac{\partial E_s}{\partial t}\left(\frac{\partial f}{\partial t}-w\right)\left(\cos(\Psi),-\sin(\Psi),0\right) + \frac{1}{k}E_s\left(-\sin(\Psi),-\cos(\Psi),0\right)\left(\frac{\partial f}{\partial t}-w\right)^2 \tag{4.41}$$

Using the assumption of a slowly varying optical phase and amplitude in time and space, $\frac{\partial E_s}{\partial z} << kE_s$ , $\frac{\partial E_s}{\partial t} << kf$ , $\frac{\partial f_s}{\partial z} << wE_s$ , and $\frac{\partial f_s}{\partial t} << wf$

the second order derivatives become negligible and are dropped from equations 4.40 and 4.41. Using equations 4.40 and 4.41, equation 4.37 can be written as

$$\left(\nabla^2 - \frac{1}{c^2}\frac{\partial^2}{\partial t^2}\right)\vec{A} = 2\left(\frac{\partial E_s}{\partial z} + \frac{1}{c}\frac{\partial E_s}{\partial t}\right)\big(\cos(\Psi), -\sin(\Psi), 0\big)$$
$$+2E_s\left(\frac{\partial f}{\partial z} + \frac{1}{c}\frac{f}{\partial t}\right)\big(-\cos(\Psi), -\sin(\Psi), 0\big) = -\frac{4p}{c}\vec{J}_\perp. \tag{4.42}$$

Equation 4.42 can be simplified further by using a coordinate transformation $z_n = z + ct$, and dimensionless time $t = ct/L$ so that

$$\frac{\partial}{\partial z} + \frac{1}{c}\frac{\partial}{\partial t}$$

transforms to

$$\frac{1}{c}\frac{\partial}{\partial t} = \frac{\partial}{L\partial t}$$

making equation 4.42 become

$$2\left(\frac{1}{L}\frac{\partial E_s}{\partial t}\right)\big(\cos(\Psi), -\sin(\Psi), 0\big) + 2E_s\left(\frac{1}{L}\frac{f}{\partial t}\right)\big(-\cos(\Psi), -\sin(\Psi), 0\big) = -\frac{4p}{c}\vec{J}_\perp. \tag{4.43}$$

The transverse current density $\vec{J}_\perp$ is the sum of the individual electron currents

$$\vec{J}_\perp = -ec\sum_i \vec{b}_\perp d^3(\vec{x} - \vec{r}_i) \tag{4.44}$$

where $d^3(\ldots)$ is the three dimensional Dirac delta-function and $\vec{r}_i$ is the position of the $i^{th}$ electron. Inserting equation 4.24 for $b_\perp$ into equation 4.44, we get

$$\sum_i \frac{-K}{g}(\cos(k_0 z),\ \sin(k_0 z),\ 0)d^3(\vec{x} - \vec{r}_i). \tag{4.45}$$

Equation 4.43 can now be decoupled into two separate equations,

$$\frac{\partial E_s}{\partial t} = -\frac{2p\,eLK}{g}\sum_i d^3(\vec{x} - \vec{r}_i)\Big[\big(\cos(\Psi), -\sin(\Psi), 0\big) \bullet \big(\cos(k_0 z), \sin(k_0 z), 0\big)\Big] \tag{4.46}$$

and

$$\frac{\partial f}{\partial t} = \frac{-2p\,eKL}{g\,E_s} \sum_i d^3(\vec{x} - \vec{r}_i)\left[(-\cos(\Psi), -\sin(\Psi), 0) \bullet (\cos(k_0 z), \sin(k_0 z), 0)\right]. \qquad (4.47)$$

Upon completion of the dot product of the terms inside the brackets, the equations become

$$\frac{\partial E_s}{\partial t} = -\frac{2p\,eLK}{g} \sum_i d^3(\vec{x} - \vec{r}_i)\cos(z + f), \qquad (4.48)$$

and

$$\frac{\partial f}{\partial t} = \frac{-2p\,eKL}{g\,E_s} \sum_i d^3(\vec{x} - \vec{r}_i)\sin(z + f) \qquad (4.49)$$

where $z = (k+k_0)z - wt$.

Assuming a constant density of electrons over the small volume element being considered, and using the average phase of the potential over the volume, the summation over i electrons can be written as

$$\sum_i d^3(\vec{x} - \vec{r}_i)\cos(z + f) = r_e \langle \cos(z + f) \rangle, \qquad (4.50)$$

and

$$\sum_i d^3(\vec{x} - \vec{r}_i)\sin(z + f) = r_e \langle \sin(z + f) \rangle, \qquad (4.51)$$

where the average is denoted by $\langle .. \rangle$ and $r_e$ is the electron density. Using these relations, equations 4.48 and 4.49 become

$$\frac{\partial E_s}{\partial t} = -\frac{2\,p\,e\,L\,K\,r_e}{g} \langle \cos(z + f) \rangle, \qquad (4.52)$$

and

$$E_s \frac{\partial f}{\partial t} = -\frac{2\,p\,e\,K\,L\,r_e}{g} \langle \sin(z + f) \rangle. \qquad (4.53)$$

These two equations can be formed from the real and imaginary parts of

$$\frac{\partial}{\partial t}\left(E_s\ \mathrm{e}^{if}\right) = -\frac{2p\ \ eKLr_e}{g}\left\langle \mathrm{e}^{-iz}\right\rangle . \tag{4.54}$$

Multiplying both sides of equation 4.54 by $4peNKL/g^2mc^2$ gives

$$\frac{\partial}{\partial t}\left(\frac{4p\ eNKLE_s}{g^2 m_e c^2}\ \ \mathrm{e}^{if}\right) = -\frac{8p^2\ \mathrm{e}^2\ \mathrm{N}K^2\ L^2\ r_e}{g^3 m_e c^2}\left\langle \mathrm{e}^{-iz}\right\rangle . \tag{4.55}$$

By defining the dimensionless optical field, $a$, and the dimensionless current, $j$ as

$$a = |a|\mathrm{e}^{if}\ \ ,\ \ |a| = \frac{4p\ eNKLE_s}{g^2 m_e c^2}\ \text{ and }\ j = \frac{8p^2\ \mathrm{e}^2\ \mathrm{N}K^2\ L^2\ r_e}{g^3 m_e c^2},$$

equation 4.56 can be rewritten as the optical wave equation,

$$\frac{\partial}{\partial t}a = \dot{a} = -j\left\langle \mathrm{e}^{-iz}\right\rangle . \tag{4.56}$$

The optical wave equation shows that the optical wave is dependent upon both current and average electron phase. With no current and/or no electron bunching, the optical wave will not change.

**D. GAIN**

The FEL oscillator exchanges energy from the electron beam to the optical beam over many passes, and can operate at low gain. Gain $G$ is the fractional power change in the optical field per pass through the undulator,

$$G = \frac{a_1^2 - a_0^2}{a_0^2} \tag{4.57}$$

where $a_0$ is the optical field strength at the beginning of the undulator ($t$ = 0)and $a_1$ is the optical field at the end of the undulator ($t$ = 1). The electron beam must lose energy to the optical wave to achieve gain, thus one method to analyze gain is to determine the change in energy of the electrons. The energy of an electron is proportional to the electron phase velocity $v$ given in equation 4.36 as

$$v = \dot{z} = (k + k_0)b_z c - w\ , \tag{4.36}$$

or using dimensionless time τ where ¶$t$ =$(c/L)$ ¶$t$,

$$v = \dot{z} = L[(k + k_0)b_z - k]. \tag{4.58}$$

Using the approximation that $k+k_0 \gg k$ (since $k_0 << k$), the change in the electron phase velocity is

$$\Delta v = L\ k\ \Delta b_z. \tag{4.59}$$

Using the resonance condition of equation 4.6, one can obtain the relation

$$\Delta v = 2\ p\ N\left(\frac{2g^2}{1+K^2}\right)\Delta b_z. \tag{4.60}$$

By using equation 4.26 in a difference form , and solving for $Db_z$ we get

$$\frac{\dot{g}}{g} = \frac{g^2\ b_z\ \dot{b}_z}{\left(1+K^2\right)} \qquad \Rightarrow$$

$$\Delta b_z = \frac{\Delta g\left(1+K^2\right)}{g^3\ b_z}. \tag{4.61}$$

Substituting into equation 4.60 and using the approximation that $b_z \approx 1$, we get a relationship between $\Delta v$ and $\Delta g$ ,

$$\Delta v = 4\ p\ N\frac{\Delta g}{g}. \tag{4.62}$$

The number of electrons in a small volume $dV$ of an optical wave is given by $N_e = r_e F dV$ where $F$ is the filling factor. The filling factor is defined as the cross-sectional area of the electron beam divided by the cross-sectional area of the optical beam. Using equation 4.62, the average change of energy for an electron inside the undulator is

$$\Delta\bar{g}\ m_e\ c^2 \approx \frac{g\ m_e\ c^2\left(\langle v\rangle - v_0\right)}{4\ p\ N}. \tag{4.63}$$

The energy contained in the volume $dV$ is given by [21]

$$de_{O-beam} = \frac{E_s^2}{4p}dV. \tag{4.64}$$

Using the above relations, gain in the optical field is

$$G = \frac{de_{e-beam}}{de_{O-beam}} = -\frac{(r_e F dV) g\ m_e\ c^2 \left(\langle v \rangle - v_0\right) / (4\ p\ N)}{2E_s^2 dV / (8p)}. \tag{4.65}$$

Using the dimensionless parameter $j$, equation 4.65 can be simplified to

$$G = \frac{2\ F\ j}{a_0^2} \langle v_0 - v \rangle. \tag{4.66}$$

In weak fields, the changes in the electron phase, optical phase, and optical field are small so we can use the approximation that $\overset{\circ}{a} \approx 0$. Using the initial conditions $v(0) = v_0$, $a(0) = a_0$, and applying perturbation theory, it can be shown that

$$\begin{aligned} v = v_0 + \frac{a_0}{v_0^2}\left[\sin(z_0 + v_0 t) - \sin(z_0)\right] + \\ \frac{a_0^2}{v_0^3}\left[-\frac{1}{4}\cos(2z_0 + 2v_0 t) - \cos(2z_0) + \cos(2v_0 t) - 1 - v_0 t \sin(z_0)\cos(z_0 + v_0 t)\right] + \ldots \end{aligned} \tag{4.67}$$

To second order, the time average of the phase velocity is

$$\langle v \rangle = v_0 + \frac{a_0^2}{v_0^3}\left[2\cos(v_0 t) - 2 + v_0 t \sin(v_0 t)\right]. \tag{4.68}$$

Substituting into equation 4.66, we arrive at the low gain equation

$$G = \frac{2Fj}{a_0^2}\langle v_0 - v \rangle = \frac{jF}{v_0^3}\left[-2\cos(v_0 t) + 2 - v_0 t \sin(v_0 t)\right]. \tag{4.69}$$

In the weak field, low current approximation, the gain is shown to be primarily a function of $j$ and the initial electron phase velocity $v_0$. Figure 13 shows a plot of the gain spectrum for the range of phase velocities from –12 to 12 in a weak optical field. The curve is anti-symmetric about $v_0 = 0$ with a peak gain near 13% at an initial phase velocity $v_0 \approx 2.6$. The initial optical field is $a_0 = 1$, and dimensionless current is $j$=1.

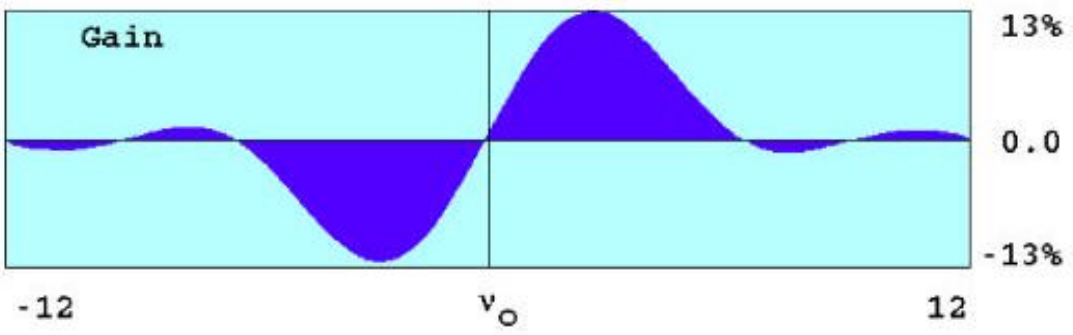


Figure 13. Single Pass Gain ($G$) versus Initial Electron Phase Velocity ($v_0$)

It should be noted that at the resonance condition $v_0 = 0$, there is no net gain. The FEL must operate slightly off resonance to have gain.

## E. PHASE SPACE

The electron phase space is a plot of the electron's phase velocity $v$ versus the electrons phase $z$. Phase space evolution is helpful in showing the evolution of the electron as it moves through the undulator from $t = 0$ to $t = 1$. The $z$ axis represents a section of the electron beam that is one optical wavelength long and is traveling at the resonance velocity $v_0$. The plotted electrons move forward (or backward) based on their relative velocity in relation to the resonance velocity.

Figure 14 shows a phase space plot for 20 sample electrons with an initial phase velocity $v_0 = 0$ and their evolution in phase space as they travel through the undulator. The electron position changes in color from yellow to red as the electron travels along the undulator. For this simulation, the electrons start out at the beginning of the undulator ($t = 0$) equally distributed in phase with an initial electron phase velocity $v_0 = 0$ (Yellow). The phase-space positions of the electrons at the end of the undulator ($t = 1$) are the final red dots for each electron. In this example, 10 sample electrons between $-\pi/2$ and $\pi/2$ increase their phase velocity (gain energy from the optical field) while the other 10 electrons between $\pi/2$ and $3\pi/2$ decrease in their phase velocity (lose energy to the optical field). The net result is that there is no net gain $G$ in optical field strength as shown in the upper right plot of Figure 14. It is clear that the electrons begin to bunch around $z = \pi/2$, which drives the optical phase, $f$, shown in the lower right plot.

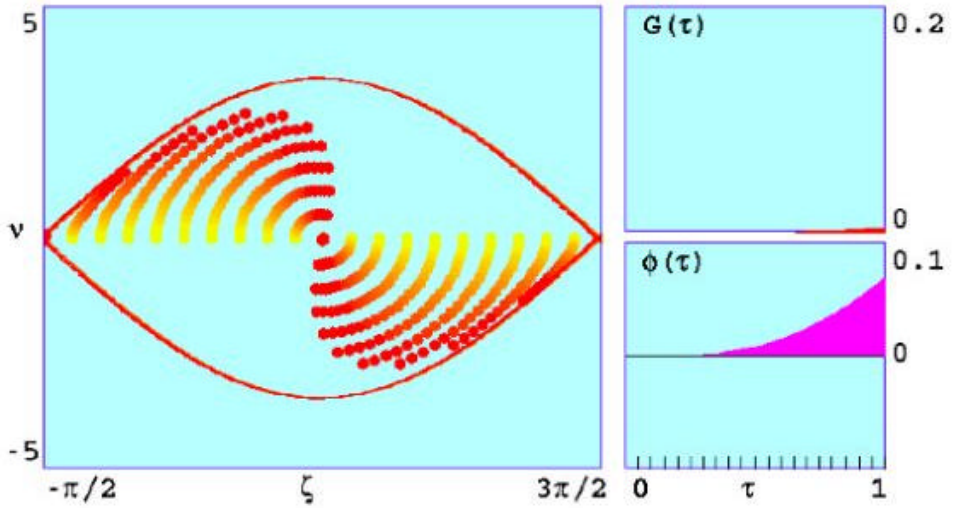


Figure 14. Phase Space Plot for a Low Gain FEL, $v_0 = 0$

As shown in Figure 13, the peak gain for a low-gain FEL occurs when the initial electron phase velocity is $v_0 \approx 2.6$. A phase space plot with $v_0 = 2.6$ is shown in Figure 15. The phase space plot shows bunching of the electrons near $z = \pi$ and shows that on average, the electrons have lowered in phase velocity thus giving a positive gain of $G \approx 13\%$.

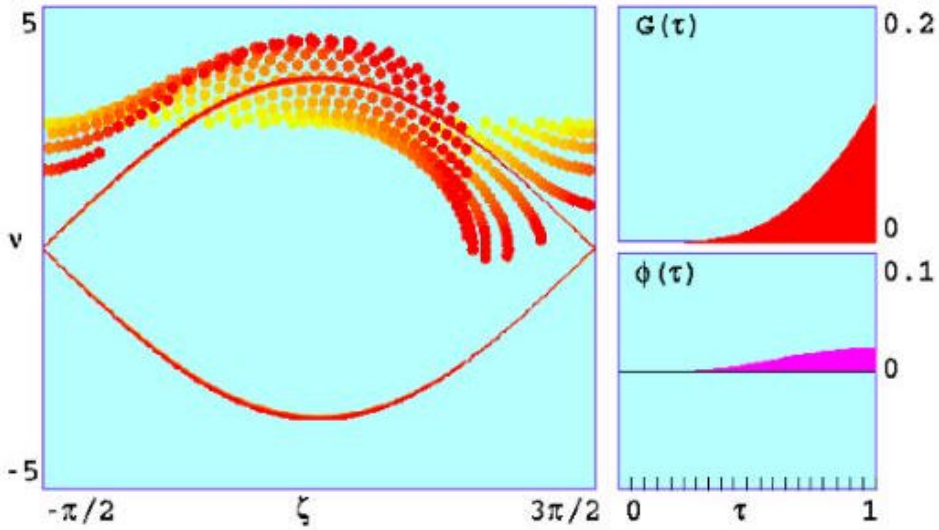


Figure 15. Phase Space Plot for a Low Gain FEL, $v_0 = 2.6$

## F. HIGH CURRENT GAIN

Equation 4.66 for a low gain FEL is only valid for weak fields $|a| << \pi$ and low current $j < \pi$. In high currents $j >> \pi$, the optical phase amplitude and phase change rapidly. Therefore the low current, low field approximation where $|a|$ is held constant and $\dot{a} = 0$ can not be used for deriving the gain. The change in the optical field and gain in a high current FEL become exponential and are given by [19]

$$|a(t)| \approx \frac{a_0}{3} e^{\left(\frac{j}{2}\right)^{1/3} \frac{\sqrt{3}t}{2}} \quad , \tag{4.70}$$

and

$$G(t) \approx \frac{1}{9} e^{\left(\frac{j}{2}\right)^{1/3} \sqrt{3}t} \quad . \tag{4.71}$$

Equation 4.71 describes high gain at resonance as a function of dimensionless time $t$ and current $j$, and is only valid for weak fields $|a| << \pi$ with high current $j >> \pi$. Figure 16 shows typical high current FEL gain and optical phase spectra.

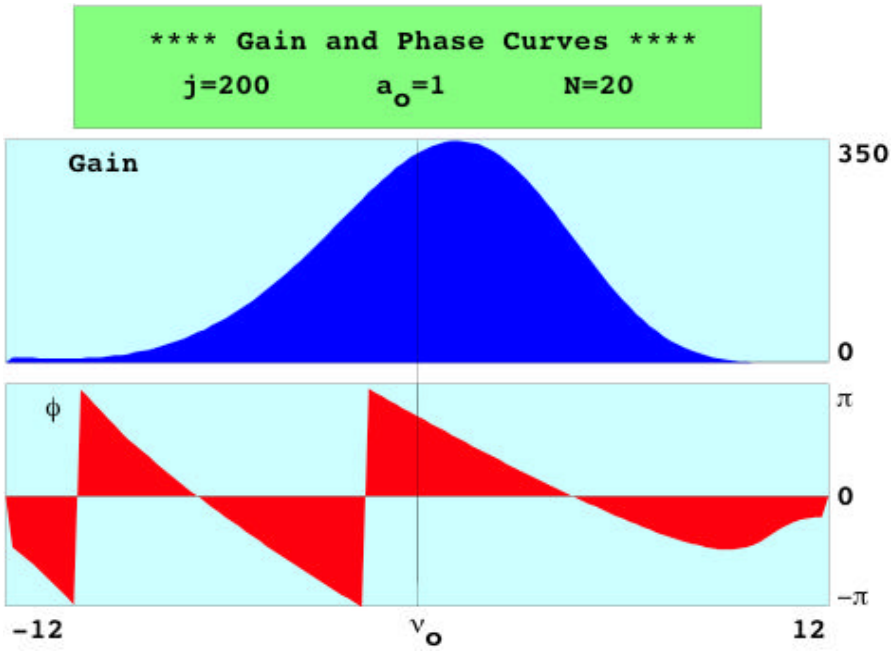


Figure 16. High current FEL gain and optical phase spectra

A phase space plot is useful in showing what happens in a high current FEL. Figure 17 shows a typical phase space evolution for a high gain FEL. An electron beam with an initial electron phase velocity $n_0 = 0$ begins to bunch near the $\zeta = \pi/2$ just as in a low current FEL. The bunching shifts the optical phase $\phi$ resulting in a shift of the separatrix back in relationship to $\zeta$ as shown in the phase space plot. As a result, maximum optical amplitude growth occurs, and gain is exponential through the remainder of the undulator. Very high gains are possible in high current operations of the FEL. A gain of $G$~350 is shown in Figure 17 as a result of an initial current $j$=200 in a weak field of $a_0$=1.

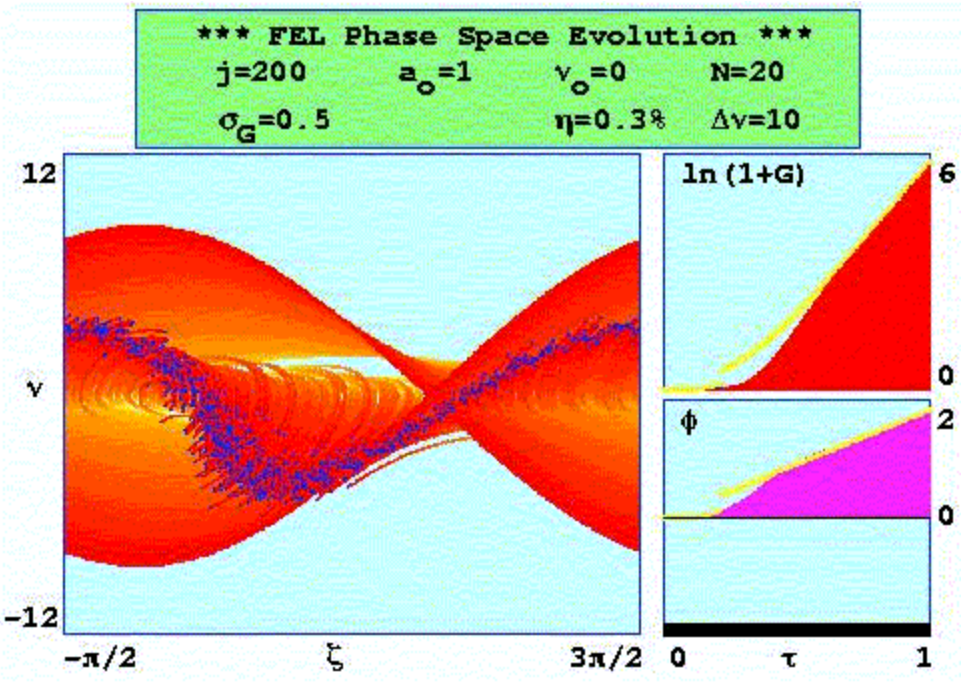


Figure 17. High Gain FEL Phase Space Evolution

# V. SIMULATION OF A SHORT RAYLEIGH LENGTH FEL

## A. INTRODUCTION

In a low gain FEL, the cavity mirrors determine the fundamental optical mode, typically a Gaussian shape. At the narrowest part of the optical beam, the beam waist radius $W_0$ is typically only a few millimeters and is usually located at the center of the undulator [23]. The beam radius will spread due to diffraction as it propagates in the $z$ direction according to

$$W^2 = W_0^2\left(1+\left(\frac{z}{Z_0}\right)^2\right), \tag{5.1}$$

where z is the displacement from the beam waist along the undulator axis, $Z_0 = \delta W_0^2/l$ is the characteristic spreading distance, called the Rayleigh length, and is the distance from the waist over which the beam waist area doubles. Transverse dimensions are normalized to $\sqrt{Ll/p}$ and longitudinal dimensions normalized to undulator length $L$. Thus, the normalized Rayleigh length is $z_0 = Z_0/L$ and the dimensionless waist $w = W\sqrt{Ll/p}$ . Equation 5.1, written in dimensionless terms, where $z = (t - 1/2)L$, becomes

$$w = \sqrt{z_0 + (t-1/2)^2 / z_0}\ . \tag{5.2}$$

The FEL is capable of producing extremely high average and peak power densities. The average electron beam intensities can be hundred's of MW/cm$^2$ and the intensity of the optical beam in the FEL can approach these intensities [22]. No mirror or optical material can withstand such high power densities without extensive damage. Therefore, the optical beam radius $W$ must expand before reflecting on mirror surfaces to decrease the intensity on the cavity mirrors to acceptable levels. As shown by equations 5.1 and 5.2, the spot size on the mirrors can be increased by either lengthening the optical cavity, and/or by shortening the Rayleigh length. For applications where space is limited, a short Rayleigh length is an attractive alternative to lengthening the cavity.

The TJNAF proposed 100 kW FEL will operate with an electron beam power of 14 MW, thus requiring an extraction efficiency of 0.7% to reach the 100 kW output. Table 2 lists the proposed parameters for the 100 kW FEL.

| Parameter | Symbol | Value |
|---|---|---|
| Electron Beam Energy | $E_e$ | 210 MeV |
| Pulse Repetition Rate | $\Omega$ | 750 MHz |
| Peak Current | $I_{pk}$ | 270 A |
| Electron Pulse length | $l_e$ | 0.1 mm |
| Electron Beam Radius | $r_e$ | 0.3 mm |
| Undulator wavelength | $\lambda_0$ | 8 cm |
| Undulator Periods | N | 36 |
| Undulator length | L | 288 cm |
| Undulator Parameter | K | 1.7 |
| Optical Wavelength | $\lambda$ | $\approx$ 1μm |
| Cavity Length | S | 32 m |
| Resonator Quality Factor | Q | 4.2 |

Table 3. TJNAF 100 kW Parameters

The resonator quality factor Q = 4.2 corresponds to a mirror transmission output of 1/Q ≈20 %. Thus for a 100 kW output power there are 500 kW of optical power

impinging on each mirror. The power densities on the mirrors were calculated for the TJNAF FEL with dimensionless Rayleigh lengths of $z_0$ = 0.1, 0.2, 0.3, 0.4, and 0.5. Figure 18 shows the optical modes and mirror power densities on the mirrors for these different Rayleigh lengths. Reducing the Rayleigh length from $z_0$ = 0.5 to $z_0$ = 0.1 lowers the power density on the mirrors by 500 %.

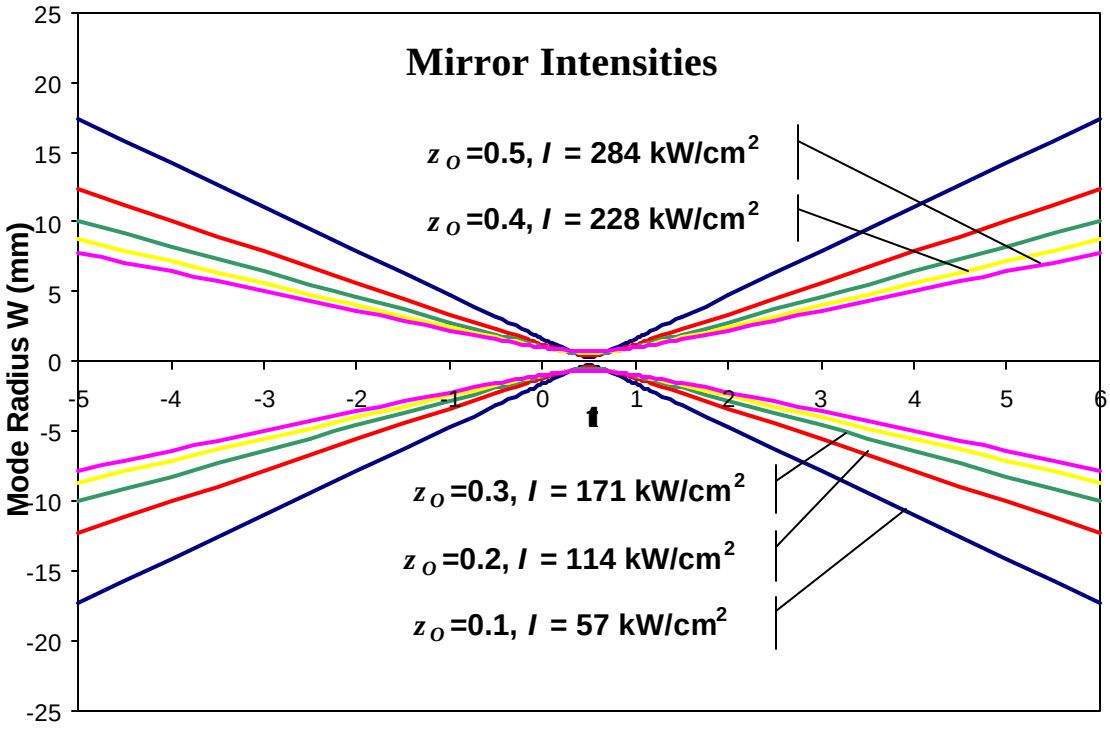


Figure 18. Mode Shapes and Mirror Intensities for Various Rayleigh Lengths

In support of the proposed 100 kW FEL upgrade for TJNAF, numerous multimode simulations were run to model and study the optical mode interaction with the electron beam. As the Rayleigh length changes, the optical mode shape changes. Due to resulting changes in the filling factor $F$, gain and steady-state power of the FEL may be affected. Using the pendulum equation to describe the electron motion and the optical wave equation to describe the optical field, three-dimensional ($x$, $y$, $t$) FEL simulations, were used to study these effects. Dimensionless parameters are used in the program to generalize results so they can be applied to FEL's of various specific design parameters,

minimize numerical errors, and reduce equations by combining constants into meaningful variables.

Figure 19 presents a three-dimensional simulation with a table of the dimensionless parameters for the simulation shown in the upper right hand block.

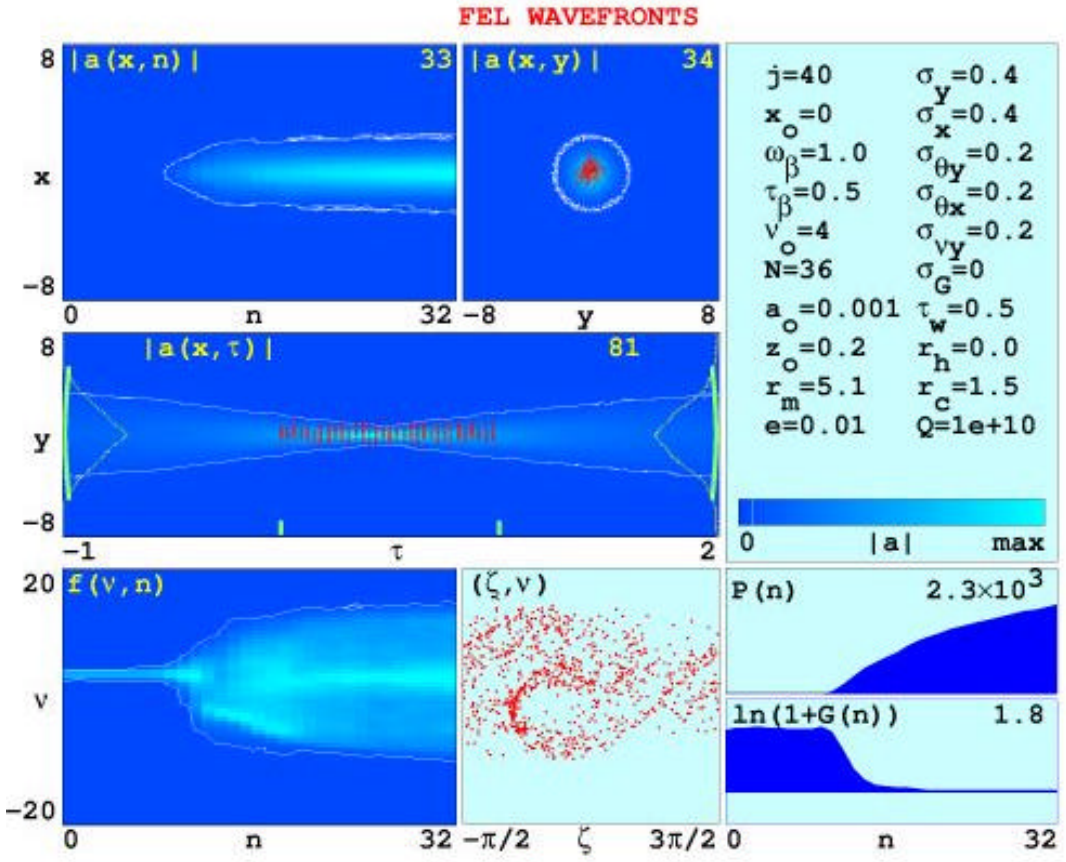


Figure 19. Three-Dimensional Simulation Results For the TJNAF 100 kW FEL

The dimensionless electron beam radius in the $x$ and $y$ dimensions is $s_x = s_y = 0.4$. The dimensionless betatron frequency is $w_b = Kk_0L/g = 1$ over the undulator length with the electron beam focused in the middle of the undulator at $t_b = 0.5$. Betatron motion describes the electron motion over many periods in the undulator with no light present and is given as

$$y(t) = y_0 \cos(w_b t) + \frac{Lq_y}{w_b} \sin(w_b t) \tag{5.3}$$

where $y_0$ and $q_y$ are the initial position and injection angle of the electron as it enters the undulator relative to the undulator axis $z$.[23] The beam's angular spread $s_{qx} = s_{qy} = 0.16$ (rounded to 0.2 in figure) is determined using the matching requirement that $s_{qy} = w_b^2 \, s_y^2$ and is comparable with constant emittance results. The Rayleigh length for this simulation is $z_0 = 0.2$

The plot in the upper left of Figure 19, $|a(x,n)|$, tracks the development of the optical mode over n=32 passes and shows how the optical mode develops in the cavity. The top center plot, $|a(x,y)|$, presents the wavefront cross-section as it exits the undulator at $\tau = 1$, and shows the electron beam (red) centered in the wavefront. The center plot, $|a(x,t)|$, is a cross-section of the optical mode in its final pass. The electron beam is shown in the undulator at each program iteration. In this simulation,to reduce computation time, the mirror separation was shortened to three times the undulator length instead of the actual separation of 11 times the undulator length. This does not change the result as the additional resonator length does not contribute to the optical field. The lower left plot, *f(v,n)*, presents the electron phase velocity distribution and how it changes over 32 passes. The final electron phase-space plot is presented in the lower center plot and shows a final spread of $Dv = 24.5$ which corresponds to an energy spread of $Dg/g = 5.4\%$ . The bottom right hand corner shows the development of gain *G(n)* and optical power *P(n)*. Gain and power evolution are the parameters of interest for the simulations presented in the next two sections.

## B. WEAK FIELD GAIN SIMULATIONS

Weak field gain simulations give insight into how a FEL will start up from a cold cavity. Simulations were conducted for the proposed TJNAF FEL with variations of Rayleigh length from $z_0 = 0.1$ to 0.5, electron beam radius from $s_x = s_y = 0.1$ to 0.5, and initial electron phase velocity from $v_0 = 1$ to 15. Due to the large number of simulations required, the work was divided among several people, my contribution consisting of all simulations for Rayleigh lengths $z_0 = 0.1$, 0.2 and analysis of data. Figure 20 shows a plot of gain $G$ versus initial electron phase velocity $v_0$ for the Rayleigh lengths of $z_0 = 0.1$, 0.2, 0.3, 0.4, and 0.5 with an electron beam radius of $s_x = s_y = 0.3$. Peak gain for

Rayleigh lengths $z_0$ = 0.1 to 0.4 occurred at an initial electron phase velocity of $v_0$ = 4 and the peak for $z_0$ = 0.5 was at $v_0$ = 3.

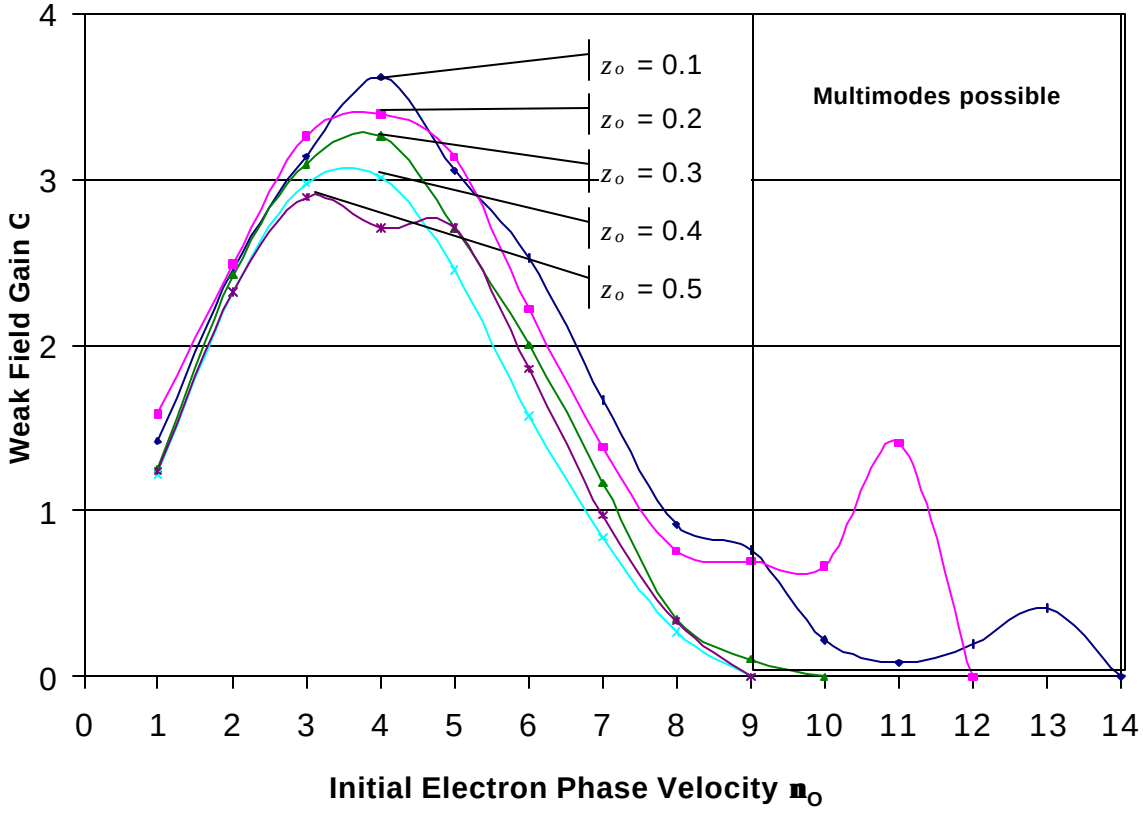


Figure 20. Weak Field Gain vs Initial Electron Phase Velocity

The general trend of decreasing gain at higher phase velocities was broken for shorter Rayleigh lengths due to multiple optical modes that supported increased gain at higher phase velocities. Similar results were obtained for electron beam sizes $s_x = s_y$ = 0.1, 0.2, 0.4, and 0.5.

Figure 21 shows a summary of weak field gain versus electron beam radius at the optimum electron phase velocity for Rayleigh lengths of $z_0$ = 0.1, 0.2, 0.3, 0.4, and 0.5.

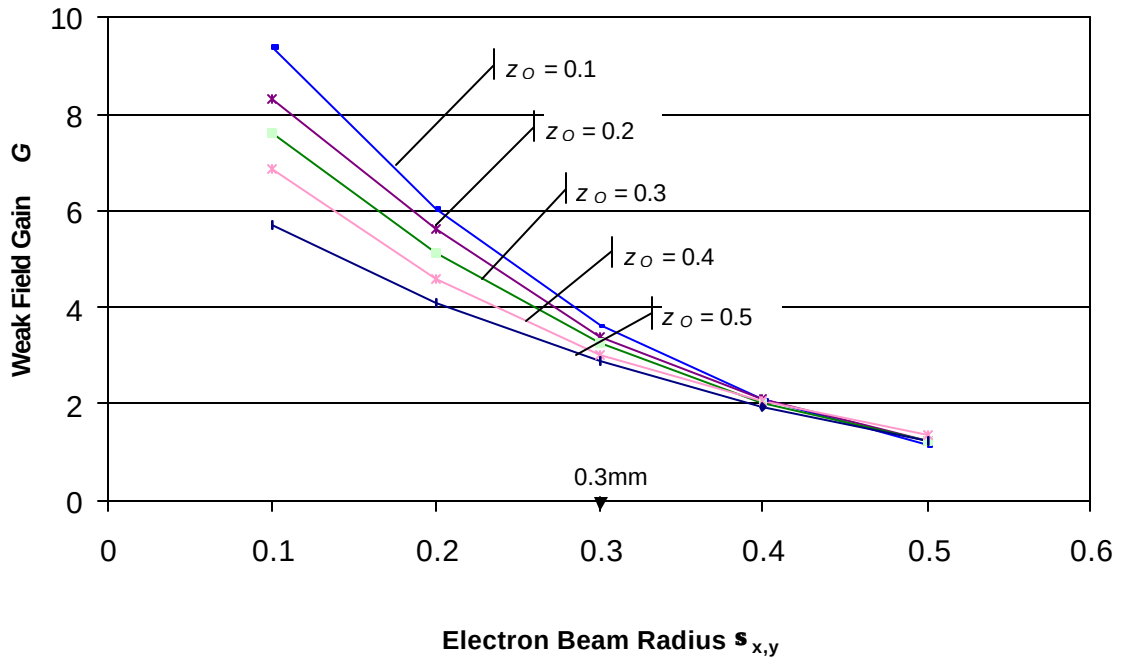


Figure 21. Weak Field Gain vs Electron Beam Radius

As the electron beam radius is increased, gain decreased in all cases due to the increased number of electrons being outside the optical mode, reducing the gain. The combination of a small electron beam radius and short Rayleigh length increases the electron beam density causing amplification of the optical mode and increasing the gain. Results from these simulations show that shorter Rayleigh lengths with small electron beam radius do not adversely affect weak field gain – in fact, they enhance it.

## C. STEADY STATE POWER SIMULATIONS

The weak field gain simulations showed that the short Rayleigh length FEL has good gain and therefore will build optical power from the initial cold cavity with no initial optical field. The next step is to determine the final steady state power $P$ achievable and the corresponding FEL efficiency $h$. Simulations for the proposed TJNAF 100 kW FEL were conducted by varying the Rayleigh length from $z_0$ = 0.1 to 0.5, the electron beam radius from $s_x = s_y$ = 0.1 to 0.5, and the initial electron phase velocity from $v_0$ = 1 to 15 to determine final power and efficiency reached for each of the

combinations. These simulations use a strong initial optical amplitude to shorten program run time. It has already been shown in the last section that weak field gains will build the optical field from cold cavity. Figure 22 is a plot of the FEL efficiency $h$ versus initial electron phase velocity $v_0$ for five different Rayleigh lengths ranging from $z_0$ = 0.1 to 0.5.

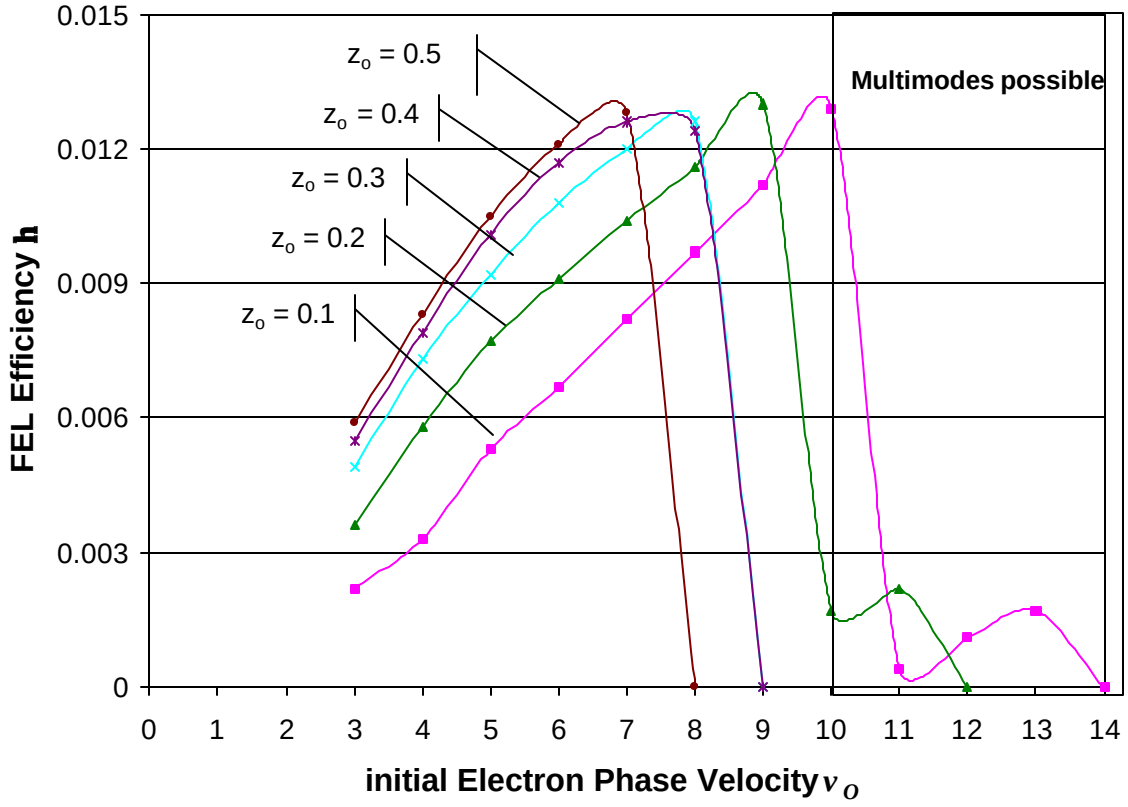


Figure 22. FEL Efficiency vs Initial Electron Phase Velocity

To understand how the electron beam radius affects efficiency, the highest peak power for each value of Rayleigh length (at the optimum initial phase velocity for that Rayleigh length) was plotted against the electron beam radius. Figure 23 shows a plot of the FEL efficiency versus the electron beam radius.

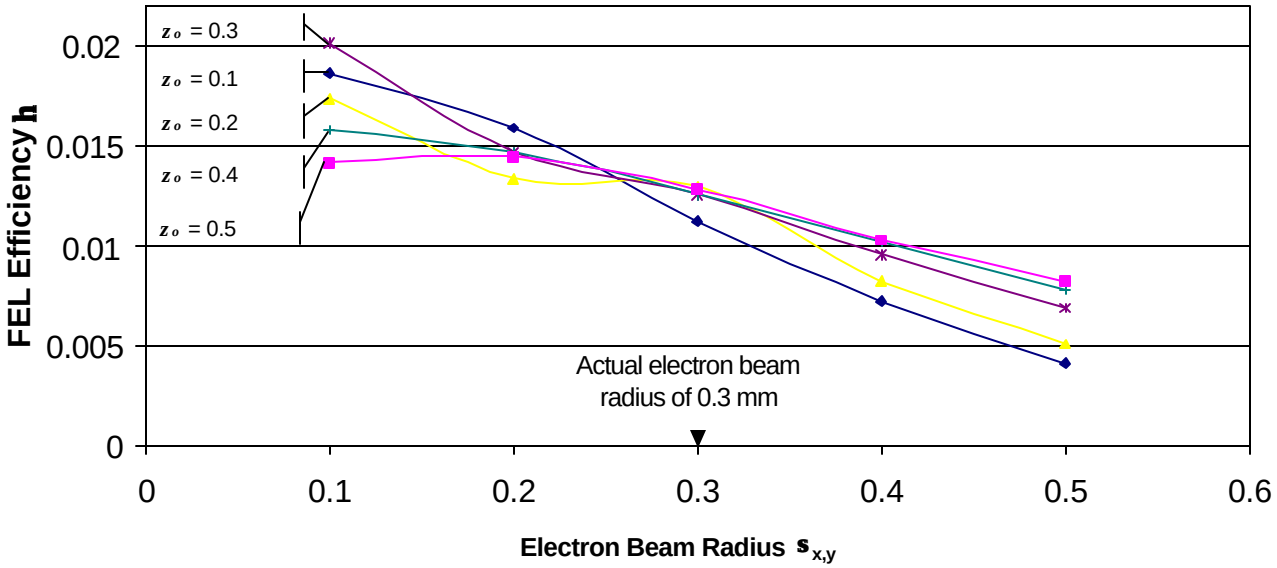


Figure 23. FEL Efficiency vs Electron Beam Radius

Figure 23 shows that the FEL efficiency increases as the electron beam radius decreases. This increase is due to concentration of the electrons within the optical mode. Figure 24 shows the maximum efficiency obtained for each Rayleigh length.

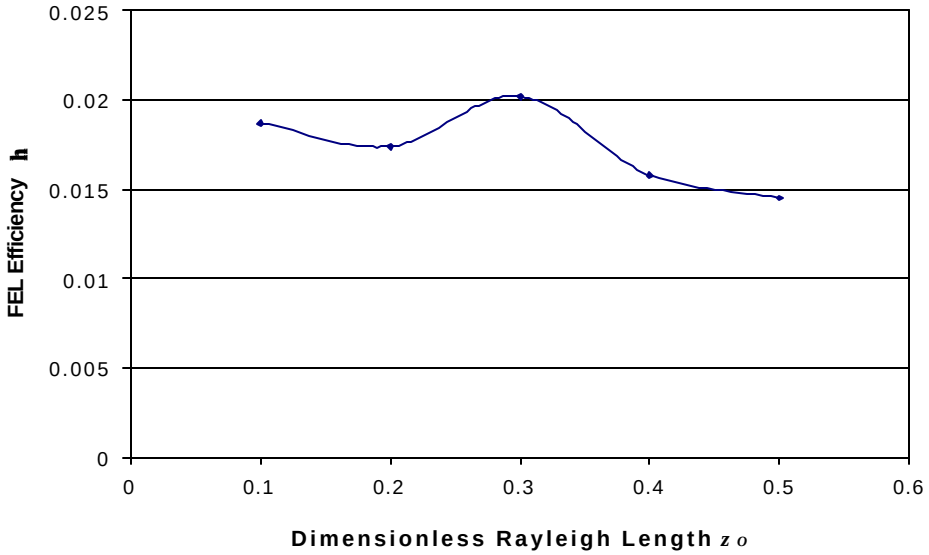


Figure 24. FEL Efficiency vs Rayleigh Length

In Figures 23 and 24, it is clear that the maximum efficiency for the FEL occurs at a Rayleigh length of $z_0$ = 0.3. This agrees with the predicted optimum filling factor occurring at $z_0 = 1/(2\sqrt{3}) \approx 0.3$ due to optimization of mode volume [19]. The maximum efficiency was 2% with a dimensionless electron beam radius of $s_x = s_y = 0.1$, and the initial electron phase velocity $v_0$ = 11 for $z_0$ = 0.3.

With a short Rayleigh length and small electron beam radius, multimode oscillations were observed with steady-state power oscillating as much as 20%. Figure 25 shows a short Rayleigh length simulation exhibiting multimode oscillations.

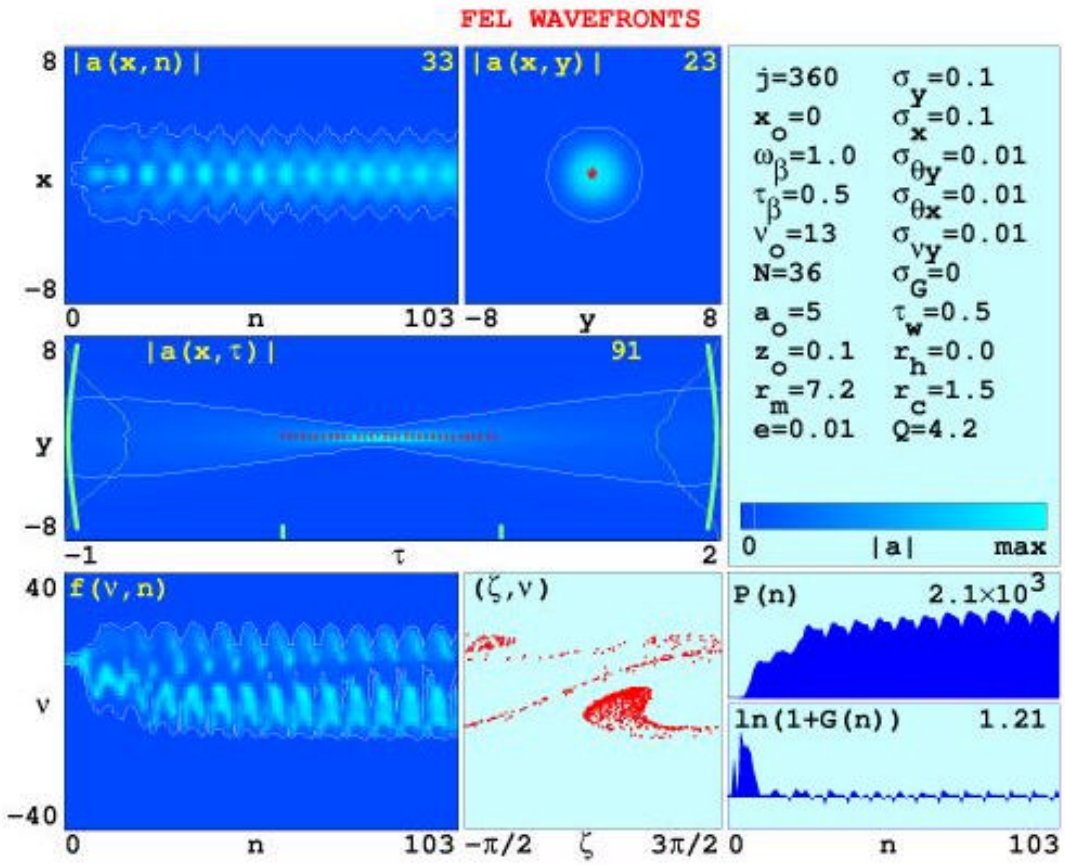


Figure 25. Multimode Oscillation Example

The oscillations are clearly visible as the modes compete resulting in an oscillating power at steady state conditions. The resulting efficiency, even with oscillations, is still greater than the required 0.7% for an output of 100 kW.

Based on the simulations, an FEL utilizing a short Rayleigh length provides sufficient gain and efficiency for 100 kW and greater operation, and allows for the power density at the mirrors to be reduced, thus preventing mirror damage. A short Rayleigh length design may be a step towards a compact high power FEL suitable for use as a shipboard weapon system.

THIS PAGE INTENTIONALLY LEFT BLANK

# VI. MIRROR VIBRATION AND FEL STABILITY SIMULATIONS

## A. INTRODUCTION

In the previous section it was shown that short Rayleigh length FELs could operate with sufficient gain and efficiency to produce an output of 100 kW or greater for the proposed TJNAF FEL. The short Rayleigh length option appears to be a step in the right direction for increasing the power of a FEL to a MW class system. But operation of an FEL at short Rayleigh lengths introduces additional problems that need to be considered. The short Rayleigh lengths are possible only when the mirrors of the optical cavity are in a nearly concentric configuration. This arrangement may make the system very sensitive to mirror vibration and misalignment. A small angular change in the mirror position could possibly drive the optical mode to rotate such that it may reduce interaction with the electron beam reducing gain and power.

To determine the effect of mirror vibration on the performance of the FEL, simulations were conducted for a proposed 1 MW FEL design. The parameters are similar to the 100 kW parameters presented in Chapter IV with the following changes. The dimensionless current is $j$ = 210, corresponding to an electron beam energy of 185 MeV with a peak current $I_{pk}$ = 3.2 kA. The electron pulse remains 0.1 mm long with a pulse repetition rate of $W$ = 750 Mhz. The resulting power in the electron beam is 143 MW, so that an extraction efficiency $h$ = 0.7% is required to achieve a 1 MW output. The dimensionless Rayleigh length is $z_0$ = 0.03 with an undulator length of $L$ = 0.6 m and cavity length of $S$ = 12 m. The optical wavelength for this design is $l$ = 1 μm.

The simulations are conducted with the mirror at a fixed rotation $q_{sim}$. A static condition can be used for the mirror since the mirror vibration frequencies are on the order of kHz, but the light only interacts with the mirror on the order of microseconds. Thus, the mirror appears to be stationary to the light pulse.

## B. OPTICAL MODE TILT

For a mirror that is tilted off the cavity's optical axis by an angle $q$, the optical mode will tilt by an amount $j$. A corresponding shift in the mode spot on the mirror is given by $dy \quad (S/2)j$. If the optical mode rotation is such that the mode no longer

contains the electron beam, the laser will not operate. Figure 26 shows a diagram of mode tilt and corresponding spot shift at the mirrors. When the spot center shifts on the order of the mode radius *(dy»w)*, the optical mode will rotate $j = j_{max}$ outside the electron beam and the laser will no longer function.

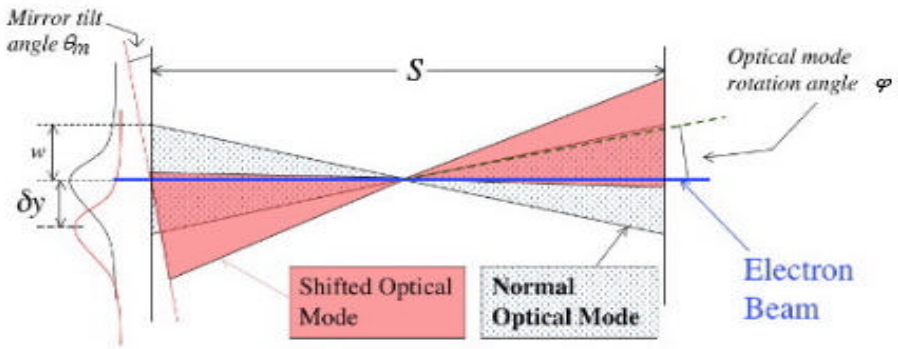


Figure 26. Optical Mode Tilt

For *dy»w*, and using the geometric estimate of $dy = (S/2) j_{max}$ and equation 5.1, it can be shown that

$$j_{\max} \approx \frac{2}{S}\sqrt{\frac{l z_0}{p}\left(1+\frac{z^2}{z_0^2}\right)}\,. \tag{6.1}$$

With $z=S/2$ and $z_0 << S$, equation 6.1 reduces to

$$j_{\max} \approx \sqrt{\frac{l}{p z_0}} \tag{6.2}$$

The optical mode tilt as a function of mirror tilt for a cold cavity (no electron beam present and thus no gain) is well known. Mirror tilt as a function of optical mode tilt is given as [26]

$$q_{cc} = (1+g)\, j \tag{6.3}$$

where $q_{cc}$ is the predicted mirror tilt for a cold cavity and the resonator parameter $g=1-S/R$ where $R = S/2 + 2Z_0^2/S$ is the mirror radius of curvature. In the limit that $Z_0 << S$, equation 6.3 becomes

$$q_{cc} \approx \left( \frac{8Z_0^2}{S^2} \right) j \ . \tag{6.4}$$

Using the parameters for the proposed 1 MW design $Z_0$ = 0.018 m and $S$ = 12 m, we see that $q_{cc}$ = 18x10$^{-6}$ $j$. Thus, a small change in the mirror tilt angle $q$ should result in a large change in the optical mode tilt.

## C. SIMULATIONS

The computer simulation used to model the mirror tilt effect on FEL performance is the same three-dimensional FEL simulation used for the power and gain simulations presented in Chapter V. The same dimensionless parameters were used in these simulations and the program was modified to incorporate a tilt to one of the mirrors by a dimensionless amount $q_m = q/(l/pL)^{1/2}$.

The dimensionless mirror tilt angle $q_m$, and the initial electron phase velocity $v_0$ are varied in the simulations with the extraction efficiency $h$ being recorded for each combination of $q_m$ and $v_0$. Figure 27 shows a sample simulation output for a dimensionless mirror tilt angle of $q_m$ = 0.25, and initial electron phase velocity of $v_0$ = 10. The actual mirror tilt angle for the simulation is $q_{sim}$ = 200 μrad with the corresponding optical mode tilt angle $j_{sim}$ = 2300 μrad. The output plots shown in Figure 27 are the same types of plots that were described in Chapter V. The optical mode rotation can be seen clearly in the center plot. Note that the axes are not to scale since the y axis covers about 10 mm and the $t$ axis covers 1.8 m. Thus, the optical mode rotation angle is greatly exaggerated. The optical mode rotation can also be seen in the top-middle plot where it is apparent that the electron beam is no longer centered in the optical mode wavefront at the end of the undulator $t$ = 1. The extraction efficiency $h$ for this extreme example of rotation was $h$ = 1.3%, and is greater than the required 0.7% for a 1 MW output.

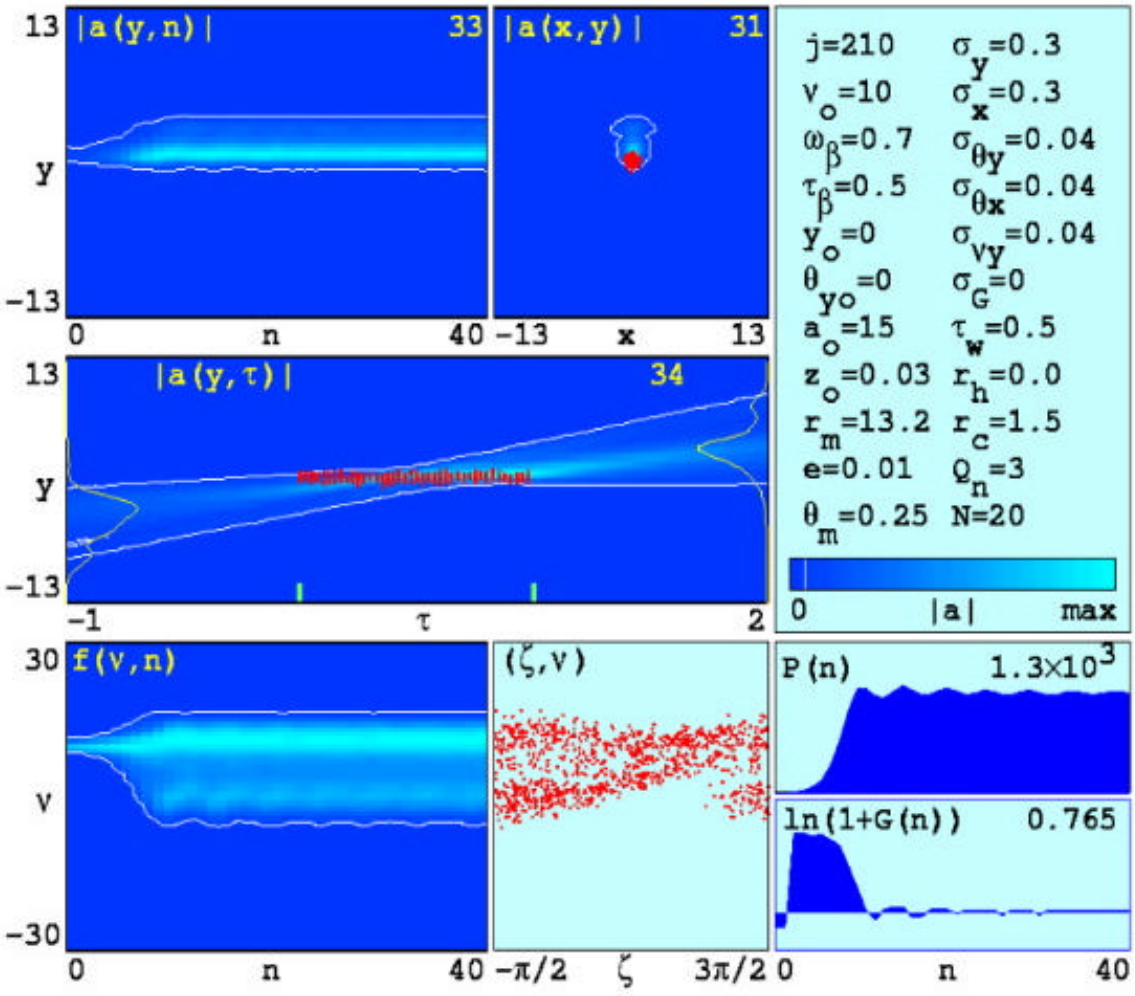


Figure 27. Mirror Tilt Simulation Results

## D. RESULTS

Figure 28 is a plot of efficiency $h$ as a function of initial phase velocity $v_0$ for mirror tilt angles $q_m$ = 0, 0.0825, 0.167, and 0.25 ($q$ = 0, 0.06, 0.12, and 0.18 mrad).

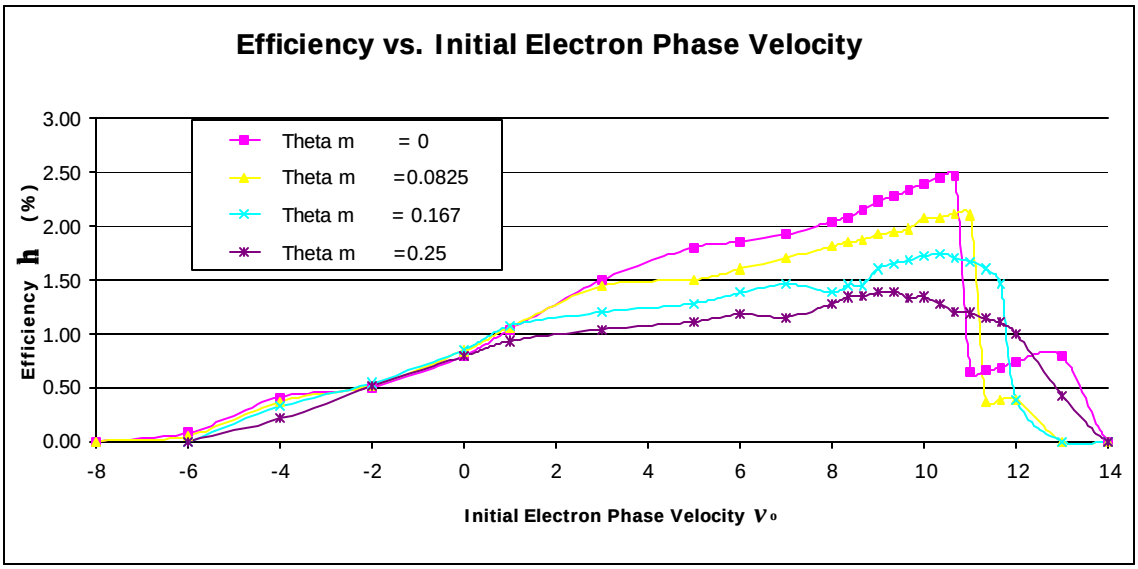


Figure 28. Efficiency vs Initial Electron Phase Velocity as a Function of Mirror Tilt $q_m$

For small mirror tilt angles, efficiency goes up as the initial electron phase velocity $v_0$ increases until $v_0 \approx 10$ where there is a sharp drop in FEL efficiency. The drop in efficiency is due to a change in the optical mode shape going from a roughly Gaussian mode to a more complicated higher order mode structure. For larger mirror tilts, the drop is not as sharp and a more gradual change between modes was seen in the simulations.

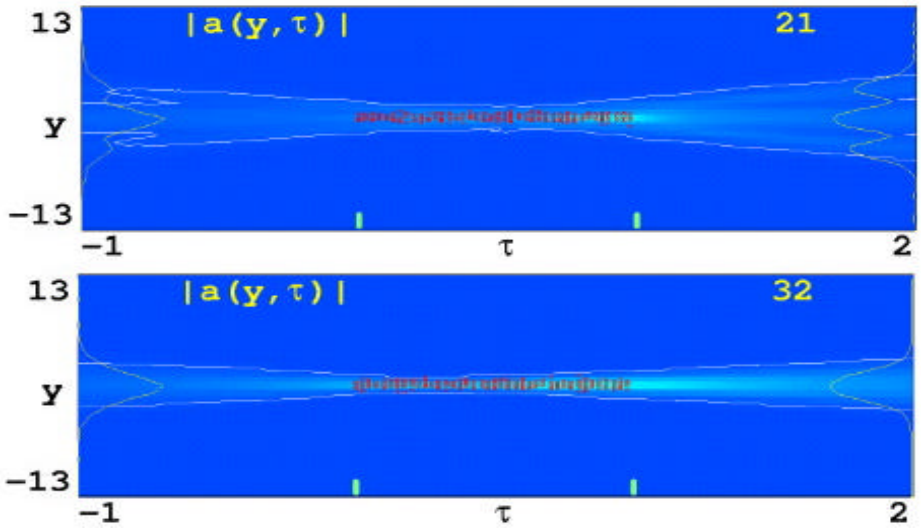


Figure 29. Gaussian mode and Higher Order Optical Modes

Figure 29 shows two cross sections for a mirror tilt of angle $q_m$ = 0.0825. The upper plot is for $\nu_0$ = 11.33 and shows a higher order optical mode at the mirrors with an extraction efficiency $h$ = 0.47 % (less than the required 0.7% for a 1 MW output). In contrast, the lower plot for $\nu_0$ = 1 shows a near Gaussian optical mode with a greater efficiency $h$ = 1.06 %, than for the higher-order mode case.

A comparison of the predicted maximum mirror tilt angle for a cold cavity $q_{cc}$ and the simulated maximum mirror tilt angle $q_{sim}$ based on the same optical mode tilt $j$ showed that the cold cavity theory predicted a much smaller mirror tilt would produce a given optical mode tilt $\varphi_0$ (i.e $q_{cc} << q_{sim}$). For an optical mode tilt of $\varphi$ = 2300 μrad, the cold cavity theory predicts a mirror tilt $q_{cc}$ = 0.04 μrad , while our simulations actually gave $q_{sim}$ = 180 μrad. This shows that the optical mode is much less sensitive to mirror tilt than cold cavity theory predicts, indicating that the electron beam plays a dominant role in determining the final optical mode tilt.

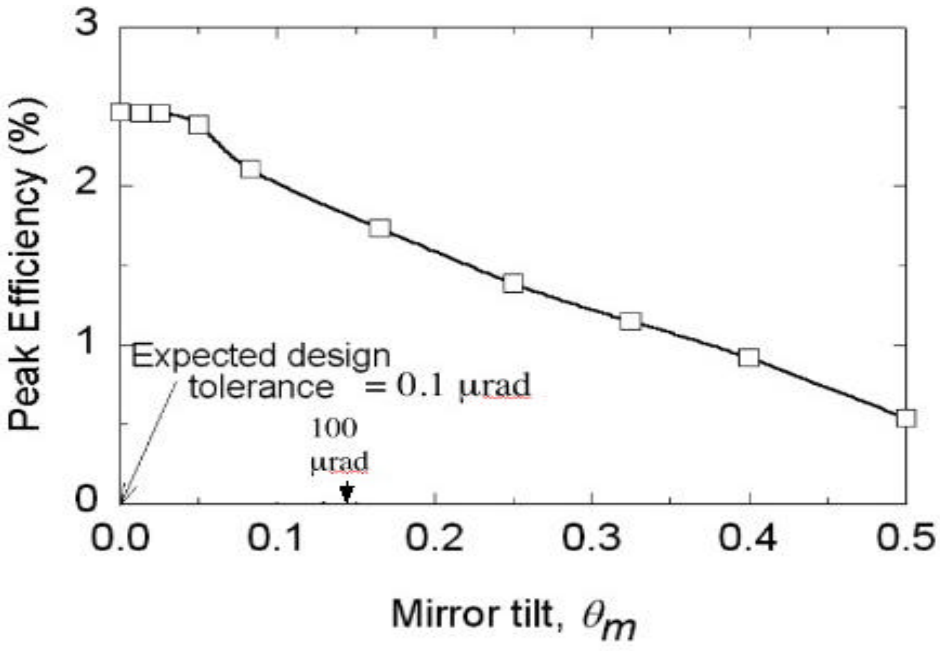


Figure 30. Efficiency vs Mirror Tilt

Figure 30 shows the FEL efficiency as a function of mirror tilt. As expected, efficiency decreases as the mirror tilt increases. For very small tilt, almost no change in

efficiency was noted. As the tilt continued to increase, the efficiency began to decrease. Even for mirror tilts as large as 290 μrad ($\theta_m$ = 0.4), the efficiency was greater than the 0.7% required for a 1 MW output. Current technology using active alignment techniques allows mirrors to be held stable to a tolerance of less than 0.1 μrad. Within this range there is clearly no noticeable change in FEL efficiency. Similar results were obtained in simulations conducted for the proposed 100 kW FEL at TJNAF [24]. Based on the results of the 1 MW and 100 kW simulations, mirror stability for a short Rayleigh length FEL does not appear to be an issue for operations when mirrors are stabilized to a maximum tilt of less than 0.1 μrad.

THIS PAGE INTENTIONALLY LEFT BLANK

# VII. POTENTIAL FEL FOR ASCM POINT DEFENSE

## A. INTRODUCTION

The research conducted for this thesis has shown that a high-power FEL using a short Rayleigh length may be possible in the future. The need for an improved ASCM point defense weapon system was motivated in the first chapter and the advantages of the FEL over other conventional weapons systems and types of lasers were discussed.

The FEL laser community is currently investigating high-power FEL's for shipboard application and taking steps to raise achievable FEL power. The TJNAF is upgrading its existing FEL to 10 kW average output and will follow up with another upgrade to a system capable of 100 kW's of average power. Several designs for scaling up to a MW class laser have been proposed and are currently being studied. There is still the question of how much power will be required to provide an adequate defense against ASCM's?

## B. REQUIRED POWER OUTPUT FOR ASCM POINT DEFENSE

Several factors must be taken into account to determine the required output power for a ASCM point defense weapon, these include (but are not limited to) the energy required to destroy the target missile, acceptable dwell time on the target (length of time laser must remain on target to deliver sufficient energy to destroy it), and the losses due to beam propagation through the atmosphere. A logical way to determine the required laser power is to start at the target and work back to the ship.

### 1. Energy Required to Destroy the Target Missile

Determining the energy needed to destroy the target is not as easy as it sounds. There are several ways that the missile can be "destroyed", by which it is meant that the missile or missile debris will not be able to strike the ship. Possible kill methods include warhead detonation, fuel tank detonation, structural damage, and sensor/guidance system interruption. Warhead detonation, fuel tank detonation, and structural damage are classified as "hard kills" because the missile is destroyed. Sensor and guidance system damage is classified as a "soft kill" since the missile is still flying, but may be unable to deliver its payload. While a soft kill will generally require less energy, a hard kill will be used as the basis for determining the energy required to destroy the target missile.

There are many different kinds of threat missiles that the FEL system must be designed to destroy, and they all may have different areas of vulnerability. The warheads and fuel tanks are located in different areas for different types of missiles and there are different types of explosive, and fuel used. To simplify the analysis, the required energy will be based on causing structural damage to the missile and allowing aerodynamic forces to destroy the missile. To cause sufficient structural damage so that the missile becomes unstable and breaks up due to aerodynamic forces, it is assumed that 0.5 liter of material must be melted. Many materials are used in the construction of modern missiles, but aluminum is often used and will be assumed in these calculations. The energy required to melt the material is given by

$$E_{melt} = r_m V_m \left( C\left(T_m - T_o\right) + \Delta H_m \right), \tag{7.1}$$

where $r_m$ is the material density, $V_m$ is the volume melted, C is the specific heat, $T_m$ is the melting temperature, $T_0$ is the initial temperature, and $\Delta H_m$ is the latent heat of melting. The values for aluminum are $r_m$ = 2.7 g/cm$^2$, C = 896 J/kg-K, $T_m$=855K, and $\Delta H_m$ = 4x10$^5$ J/kg. Assuming an initial temperature of $T_0$ = 400K, the energy required to destroy the missile is $E_{melt} \approx 2$. MJ. This calculation should be treated as an order of magnitude estimate.

The estimated energy of 2 MJ agrees with experimental data collected in conjunction with the MIRACL program, showing that tens of kW/cm$^2$ are required to destroy a missile with a dwell times of a few seconds [25]. For an average spot size on the missile of 100 cm$^2$, this gives energy in the MJ range. It will be assumed for the remainder of the calculations that about 2 MJ of energy deposited in a 100 cm$^2$ spot size is sufficient to destroy a missile. This is by no means an exact number, but it gives a ballpark estimate for discussion.

### 2. Propagation Losses

As the laser beam travels through the atmosphere, it can lose energy in several different ways. The energy can be absorbed by the atmosphere, or get scattered in different directions, or, if the column of atmosphere that the beam is going through heats up enough, thermal blooming can occur.

### *a. Absorption and Scattering*

Absorption and scattering of the laser beam are related to atmospheric conditions and will be considered in this section. The amount of energy received at the target is a fraction of the energy that is transmitted from the ship and can be described by the equation $E_{target} = T\ E_{ship}$, where $T$ is the atmospheric transmittance. The atmospheric transmittance $T$ is given by

$$T = e^{-a_e z} \tag{7.2}$$

where $a_e$ is the extinction coefficient and $z$ is the distance the light must propagate. The extinction coefficient is a sum of the absorption and scattering coefficients $a_e = a_a + a_s$ and is a function of wavelength. The scattering and absorption coefficients are dependent on the concentration and types of particles that are in the atmosphere and therefore vary greatly with different atmospheric conditions. The major contributors are $CO_2$, ozone, water, and suspended aerosols. Figure 31 is a graph of the absorption and scattering coefficients of some of the major contributors to losses as a function of wavelength [26]. (Figure 31 uses the symbol $s$ for the coefficients instead of $a$ which is used in this paper.)

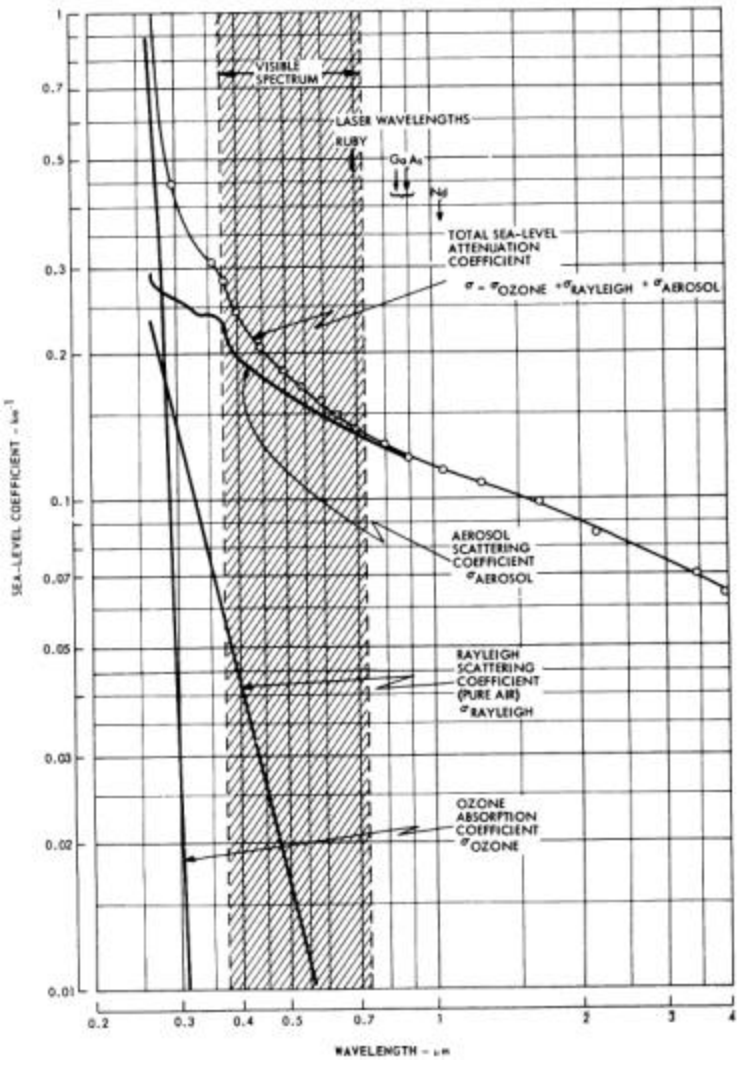


Figure 31. Extinction Coefficients vs Wavelength (from [27])

Figure 31 does not include the scattering and absorption due to water or $CO_2$. When the effects due to water and $CO_2$ are included, it becomes apparent that some wavelengths propagate much better than others. Figure 32 includes the effects of $CO_2$ and water and shows transmission windows where certain wavelengths have a much greater percent transmission than others [27].

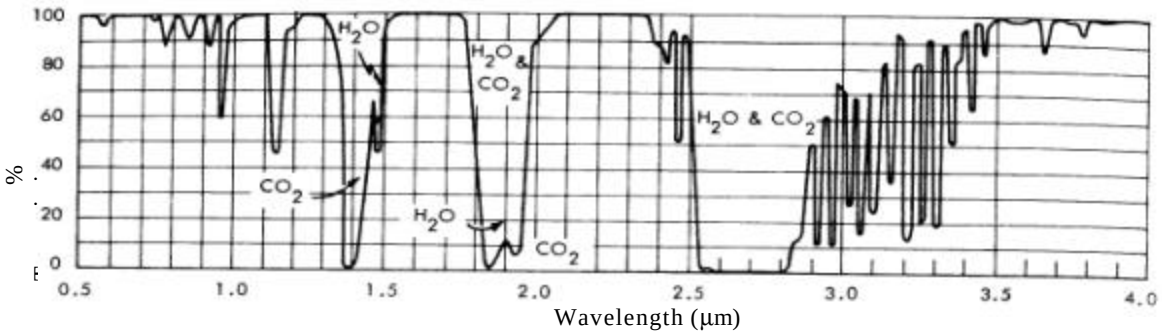


Figure 32. Percent Transmission vs Wavelength (from [27])

The ability to take advantage of these atmospheric windows of transmission using the tunability of the FEL is a great advantage over other types of lasers. For any high power laser to successfully deliver lethal amounts of energy to a target, it must operate within one of these transmission peaks. Figures 31 and 32 are for a typical atmosphere over land. A maritime atmosphere contains a much larger concentration of aerosols than the atmosphere presented in figures 31 and 32. Figure 33 shows a plot of absorption, scattering, and overall extinction coefficient as a function of wavelength for a typical maritime atmosphere [28]. The lowest extinction coefficients occur at wavelengths of 1.62, 1.25, and 1.06 μm.

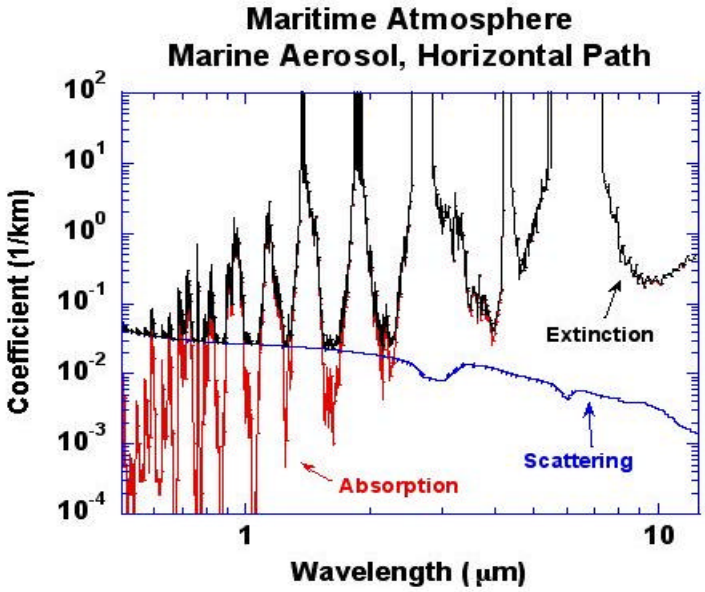


Figure 33. Coefficients of absorption, scattering, and extinction in a maritime atmosphere (from [28])

The graphs presented in this section are for a typical atmosphere in clear weather at sea level. These graphs present only a small fraction of possible conditions and can not be used to satisfactorily describe the atmospheric absorption and scattering losses for all conditions in all areas of the world. Based on current available data for scattering and absorption, the best propagation windows in order of preference appears to be the 1.62, 1.25, and 1.06 μm wavelengths, but another factor must also be considered, thermal blooming.

### *b. Thermal Blooming*

Thermal blooming occurs when the column of air through which the laser is propagating is heated causing the air to act as a diverging lens. The onset of thermal blooming is a function of the power density of the beam, absorption coefficient of the atmosphere, and the time that the laser beam is acting on the same column of air. For a given power density and atmosphere, the time until the onset of thermal blooming in a column of air is known as the critical blooming time $\tau_c$. The column of air through which the laser is propagating is continually changing due to cross winds and the slewing rate of the beam moving through the atmosphere to stay on target. One estimate used to calculate the critical blooming time shows that the critical blooming time is inversely proportional to the one third power of the product of the absorption extinction coefficient and beam intensity, $\tau_c \propto 1/(\alpha_a I)^{1/3}$. Figure 34 shows the peak transmission intensity as a function of wavelength including the effects of absorption, scattering, and thermal absorption for a crosswind of 10 m/s to account for channel clearing [28].

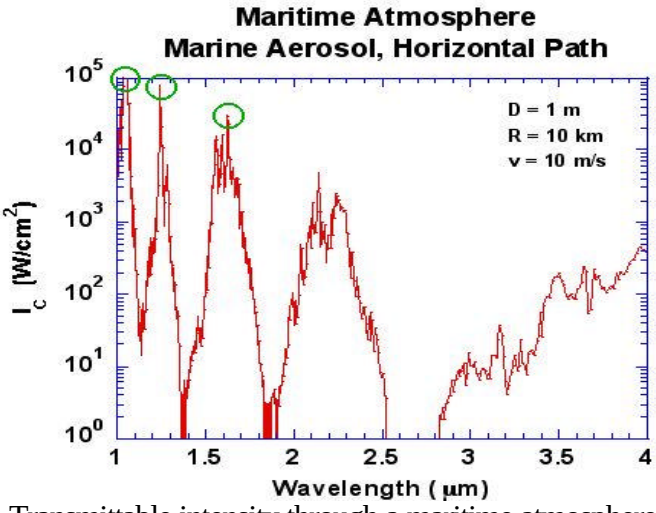


Figure 34. Transmittable intensity through a maritime atmosphere (from [28])

Figure 34 shows that the optimum transmission is at a wavelength of 1.06 μm. Referring back to Figure 33, we find a value for the total extinction coefficient is $a_e$ = 0.144 $km^{-1}$ for 1.06 μm wavelength. Figure 33 assumes a "standard clear" visibility of 23.5 km. Changes in the atmospheric visibility will cause significant changes in the value of $a$. For visibilities of 60 km (exceptionally clear day) and 8 km (light haze) the extinction coefficients are 0.042 $km^{-1}$ and 0.340 $km^{-1}$ respectively. Table 3 shows the percentage of transmitted power from the ship (% $P_{trans}$) that arrives at a target based on ranges of 1, 5, and 10 km for three different viewing conditions at the optimum wavelength of 1.06 μm.

| Viewing Conditions | % $P_{trans}$ (1km) | % $P_{trans}$ (5 km) | % $P_{trans}$ (10 km) |
|---|---|---|---|
| Exceptionally Clear (visibility = 60 km) | 95.9 | 81.1 | 65.7 |
| Standard Clear (visibility = 23.5 km) | 86.6 | 48.7 | 23.7 |
| Light Haze (visibility = 8 km) | 71.2 | 18.3 | 3.3 |

Table 4. Percent Power Transmission as Function of Range at Various Viewing Conditions

The table above demonstrates how atmospheric conditions can significantly affect the performance of the FEL. These predictions may radically change for different environments. Many maritime atmospheres contain different types and concentrations of aerosols making the propagation profile completely different than these models. The tunability of the FEL makes it ideal as a directed energy weapon in order to adjust to these propagation windows and deliver maximum energy to the target.

## C. REQUIRED LASER POWER OUTPUT

To determine the required laser power output from the ship, several isseus must be considered. What kind of dwell time is acceptable? What is the closest that I want a missile to get to the ship? How many missiles per engagement should be considered? The list goes on. To determine the laser power at the ship, the following engagement scenario and assumptions were used:

1. Engagement of two Mach 3.5 missiles with a detection range of 12 km and engagement beginning at a range of 10 km.
2. Standard clear day, $\alpha_e = 0.144$ km$^{-1}$ corresponding to a visibility of 23.5 km.
3. 2 MJ of energy "kills" the missile.
4. 0.5 seconds required for retargeting after the first missile is destroyed.
5. The last missile must be destroyed at 1000 m so that there is a less than 5% chance of fragments hitting the ship.

For the scenario listed above, the power of the laser at the ship would have to be a minimum of 1 MW. At 1 MW the first missile would be destroyed at 4.4 km with a total dwell time of 5 seconds to deliver the required 2 MJ of energy. The second missile will be destroyed at a range of 1km with a total dwell time 2.5 seconds. The difference in dwell times is due to the decreasing atmospheric losses as the missile gets closer. Figure 35 shows a plot of the energy absorbed by each missile as a function of range for a 1 MW laser.

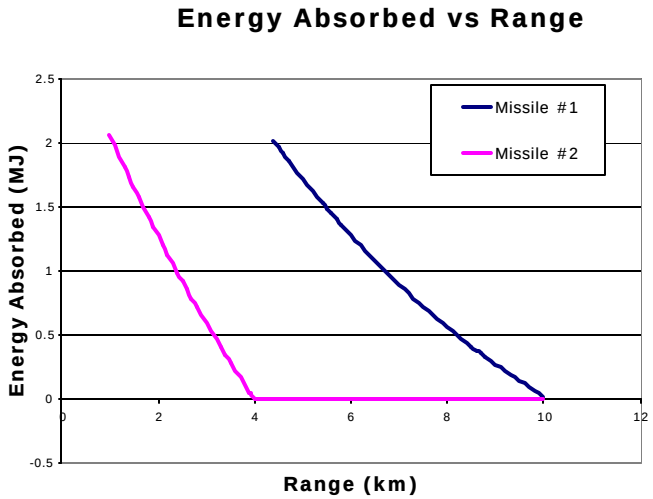


Figure 35. Energy Absorbed by Missile vs Range

It should be noted that there are many assumptions used in making this final determination of the required power for a shipboard laser. This is only intended to show order of magnitude requirements for this application, and indicates how a MW class laser is a probable solution for the growing ASCM threat.

## D. 1 MW FEL

The previous section showed that a 1 MW FEL could be a potential ASCM defense system. The system would be similar to the 100 kW FEL described in Chapter III including the electron beam control subsystem, light beam control subsystem, and auxiliary systems. However, the size of the FEL will have to scale down while power will need to scale up from current FEL's. There are several proposed MW class lasers being considered for the future. One such design was introduced in Chapter VI and simulations indicated a power output would be greater than 1 MW.

For a weapon system design to be feasible on a Navy ship, it must meet certain volume and weight limits. A comparison of the volumes and weights of three point defense weapons systems shows that the FEL is comparable in weight and volume to other systems. Table 4 shows a size and weight comparison for a FEL, Phalanx CIWS, and RAM system with a MK-49 launcher [2,3,4,9,10].

| | FEL<br>(2 Beam Directors) | PHALANX<br>(2 units) | RAM system<br>(2-MK49 launchers) |
|---|---|---|---|
| Size | FEL: 96 $m^3$<br>Beam Director:<br>16 $m^3$ each<br>Total:128$m^3$ | 57 $m^3$ each<br>Total: 114 $m^3$ | 26 $m^3$ each<br>Total: 52 $m^3$ |
| Weight | 23,000 kg<br>(estimate) | 6,170 kg each<br>Total: 12, 340 kg | Missiles: 42 @ 78.5 kg<br>3300 kg<br>Launcher: 2 @ 6117 kg<br>12230<br>Total: 15530 kg |

Table 5. Comparison of Size and Weight of Point Defense Systems

Based on the advantages a FEL offers, the estimated size and weight comparisons, and the possibility of being able to engage multiple ASCM's successfully, the MW FEL is an excellent choice for an improved point defense weapon and shows promise as a weapon system for the future.

THIS PAGE INTENTIONALLY LEFT BLANK

# VIII. CONCLUSIONS

Rapid advances in free electron laser technology are making high power FEL's possible. With the current upgrade of the TJNAF FEL to a 10 kW output scheduled for first light in March 2003, and another upgrade to an output of 100 kW scheduled to begin in 2005, high power FEL's are becoming a reality. To be a feasible weapons system capable of being deployed on Naval Combatant's, size and weight restrictions must be adhered to. One of the limiting factors for sizing considerations is the power density on the optical mirrors. To maintain the power density on the mirrors at acceptable levels, the optical cavity must be long enough to allow for diffraction. Alternatively, a short Rayleigh length may be used to cause rapid spreading of the beam. Simulations presented in Chapter V showed that by using a short Rayleigh length FEL, power densities at the mirrors are significantly reduced with no significant reduction in the power output of the FEL.

For a short Rayleigh length FEL, the resonator cavity mirrors are in a nearly concentric configuration and are sensitive to misalignment and vibration. Small vibrations of the mirror may be sufficient to cause a decrease in the performance of the FEL, and if severe enough in magnitude may prevent operation of the FEL. Simulations presented in Chapter VI showed that as mirror tilt angle increased, the FEL efficiency decreased. However, it takes a mirror tilt several orders of magnitude greater than the active alignment tolerance of 0.1 μrad before the FEL efficiency is noticeably affected. Mirror tilt, vibrations, and misalignment within achievable tolerance limits will not adversely affect the performance of a FEL.

A MW class FEL appears possible in the near future. Designing a weapon system capable of providing quicker reaction time, and speed of light delivery of lethal energy will prove to be a valuable asset for the Navy, giving ships an improved ASCM defensive capability along with surgical strike capability in the littorals. Continuation of this research is needed to advance FEL technology to the point that a shipboard weapon system is possible.

THIS PAGE INTENTIONALLY LEFT BLANK

# LIST OF REFERENCES


[1] J. Blau, T. Campbell, W. B. Colson, I. Ng, W. Ossenfort, S. V. Benson,G. R. Neil, M. D. Shinn, "Simulation of the 100 kW TJNAF FEL using a short Rayleigh length", Nuclear Instruments and Methods in Physics Research, A 483 (2002) 142-145

[2] Jane's Fighting Ships (2002-2003)

[3] Jane's Naval Weapons Systems, Online edition (2002)

a. Raytheon Phalanx CIWS

b. RIM-116A Rolling Airframe Missile

[4] United States Navy Fact File: RIM-116A Rolling Airframe Missile www.chinfo.navy.mil/navpalib/factfile/missiles/wep-ram.html, October 2002

[5] GAO Letter Report, 7/11/2000, GAO/NSAID-00-149 "Comprehensive Strategy Needed to Improve Ship Cruise Missile Defense"

[6] J.M.J. Madey, "Stimulated Emission of Radiation in Periodically Deflected Electron Beams," Journal of Applied Physics, Vol. 42, 1971

[7] L.R. Elias, W.M. Fairbank, J.M.J. Madey, H.A. Schwettman, T.I. Smith, Phys. Rev. Lett. 36,717 (1976)

[8] FAS "Mid Infrared Advanced Chemical Laser" 21 March, 1998 http://www.fas.org/spp/military/program/asat/miracl.html

[9] A. M. M. Todd, W. B. Colson, G. R. Niel, "High-Power, Compact, Free-Electron Laser Concepts"

[10] United States Navy Fact File: Phalanx Close-In Weapons System www.chinfo.navy.mil/navpalib/factfile/weapons/wep-phal.html, October 2002

[11] I. Ng, "A Free Electron Laser Weapon for Sea Archer" Master's Thesis, December 2001

[12] Byung C. Yunn, "Physics of JLAB FEL Injector" Proceedings of the 1999 Particle Accelerator Conference, New York 1999

[13] David J Griffiths, " Introduction to Electrodynamics – 3rd Edition", 1999, Prentice Hall, Upper Saddle River, NJ

[14] www.jlab.org/FEL/feldecrip.html, October 2002

[15] A. M. M. Todd, J. Rathke, H.P. Bluem, M. Cole, T. Schuheiss, et al., "High-Power Electron Beam Injector for a 100 kW Free- Electron Laser"

[16] A. M. M. Todd "FEL Brief to JTO" presented July 2002

[17] FAS "Airborne Laser", Dec. 20, 2001; www.fas.org/spp/starwars/progrm/abl.html

[18] "Airborne Laser- Technical Characteristics",

www.aeronautics.ru/nws001/abl/techspecs.html, September 2002

[19] W. B. Colson, in: W. B. Colson, C. Pelligrini, A. Renieri (Eds) *Laser Handbook*, Vol. 6., Chap. 5, Elsevier Science Publishing Co., Inc., The Netherlands, 1990

[20] W. B. Colson, "One-Body Electron Dynamics in a Free Electron Laser", Physics Letters Volume 64A, 1977

[21]. D. Jackson, "Classical Electrodynamics", Third Edition, John Wiley and Sons, New York, NY, 1999

[22] S. Benson, G. Neil, M. Shinn, "Measurements and Modeling of Mirror Distortion in a High Power FEL", SPIE, Vol. 3931B, LASE 2000, San Jose, CA, January 23-28, 2000

[23] J. Blau, "Multimode Simulations of Free Electron Lasers", Dissertation, March 2002

[24] P. P. Crooker, T. Campbell, W. Ossenfort, S. Miller, J. Blau, W. Colson, "A Study of the Stability of a High-Power Free Electron Laser Utilizing a Short Rayleigh Length", 24th International FEL Conference Proceedings, September 2002

[25] B. Anderberg, MGEN, M.L. Wolbarsht, "Laser Weapons: The Dawn of a New Military Age", Phenum Press, New York, NY 1992

[26] A. Siegman, "Lasers", University Science Books, Mill Valley, CA, 1986

[27] Solid State Division of RCA, Inc., "Electro-Optics Handbook", (1974)

[28] R. D. Stock, "Computer Simulations for a Maritime FEL", presented at 2001 Free Electron Later Development for Naval Applications Conference, (5 July 2001)

# INITIAL DISTRIBUTION LIST

1. Defense Technical Information Center
   Ft. Belvoir, Virginia

2. Dudley Knox Library
   Naval Postgraduate School
   Monterey, California

3. Dr. Fred Dylla
   TJNAF
   Newport News, Virginia

4. CDR Roger McGinnis, USN
   Naval Sea Systems Command, Code SEA 53R
   Washington Navy Yard, DC

5. Dr. George Neil
   TJNAF
   Newport News, Virginia

6. Dr. Alan Todd
   Advanced Energy Systems, Inc.
   Princeton, New Jersey

7. Dr. Gil Graff
   Office of Naval Research, Code 351
   Arlington, Virginia

8. Michael B. Deitchman
   Office of Naval Research, Code 351
   Arlington, Virginia

9. Professor William B. Colson
   Naval Postgraduate School
   Monterey, California

10. Professor Robert L. Armstead
    Naval Postgraduate School
    Monterey, California

11. Professor Peter P. Crooker
    Naval Postgraduate School
    Monterey, California

12. Professor Joseph A. Blau
Naval Postgraduate School
Monterey, California

13. Chairman, Physics Department
Naval Postgraduate School
Monterey, California

14. Lieutenant Thomas E. Campbell, USN
Naval Submarine School
Groton, Connecticut